Deficiencies of FENE dumbbell models in describing the rapid stretching of dilute polymer solutions

Indranil Ghosh, Gareth H. McKinley,[a] Robert A. Brown,

and Robert C. Armstrong[b]

Department of Chemical Engineering, Massachusetts Institute of Technology, Cambridge, Massachusetts 02139-4307

(Received 6 September 2000; final revision received 17 January 2001)

Synopsis

A wide variety of bead-spring kinetic theory models have been proposed to explain the stress growth and hysteretic behavior of dilute polymer solutions in uniaxial extension. We analyze the Kramers chain, a fine-scale model for polymer dynamics, in order to assess the validity of the coarser-grained bead-spring models in these deformations. Whereas the spring force is a simple function of the dumbbell length for the FENE spring, we find that the relationship between the ensemble-averaged end-to-end force and the extension for a Kramers chain depends on the kinematic history to which it has been subjected. In a quiescent fluid, the Kramers chain force–extension relationship is identical to the FENE force law. However, during start up of elongational flow, the ensemble-averaged end-to-end force for a given (end-to-end) length of the molecule increases with strain until steady state is reached. If the extensional flow is suddenly stopped, the Kramers chain force–extension relationship relaxes back to the FENE force–extension function. For all positive strains, the FENE dumbbell force law underpredicts the ensemble-averaged end-to-end force in the Kramers chain. For a Weissenberg number of 11.4, the end-to-end forces in the two models can differ by three to four orders of magnitude, indicating the unsuitability of the FENE dumbbell for modeling polymers in strong transient extensional flows. This paper also presents a detailed analysis of the mechanisms causing stress–birefringence hysteresis. We find that it is essential for a dumbbell model to have an end-to-end force that depends upon the deformation history in order to capture configurational hysteresis. [DOI: 10.1122/1.1357822]

I. INTRODUCTION

The advent of the filament stretching rheometer [Tirtaatmadja and Sridhar (1995)] has, for the first time, enabled quantitatively reliable measurements of transient stress growth as a function of strain and strain rate in uniaxial elongational flows of Boger fluids. The polymer concentrations of the Boger fluids were selected such that they were good approximations to dilute polymer solutions. The quality of the data has allowed direct comparisons of experiments with predictions of molecular models of polymers and has led to some interesting findings. James and Sridhar (1995) and Tirtaatmadja and Sridhar (1995) were able to elongate filaments of Boger fluids to Hencky strains as large as seven and thereby measure the steady-state elongational viscosity. In contrast to the finite,

[a]Department of Mechanical Engineering.
[b]Author to whom correspondence should be addressed; electronic mail: rca@mit.edu

steady-state extensional viscosity exhibited by the Boger fluids for a Weissenberg number Wi greater than 0.5, the Hookean dumbbell model, which is infinitely extensible, predicts unbounded stress growth. The FENE and FENE-P dumbbell models, which incorporate finite extensibility through a nonlinear spring, predict a finite extensional viscosity but underestimate the rate of stress growth at low strains [Herrchen and Öttinger (1997)]. In contrast to the response of FENE dumbbell models, Doyle and Shaqfeh (1998) demonstrated that a finer scale model, the ten-spring FENE-PM chain [Wedgewood *et al.* (1991)], describes well the experimentally observed stress growth for the first two units of Hencky strain. This analysis suggests that dumbbell models are inadequate for describing rheological behavior in the start up of an extensional flow. Doyle suggested that a dumbbell could not capture internal configurations or the conformation dependence of drag exhibited in a real polymer.

It is the goal of this paper to understand the origins of these deficiencies. More specifically, we examine whether the spring force in a dumbbell model can be a simple function of end-to-end distance, or whether it must have a more complicated form if the dumbbell model is to capture the behavior of a polymer molecule in a strongly deforming flow such as the sudden inception of a steady elongational flow. An additional objective is to understand why the FENE dumbbell model poorly describes the experimentally observed stress–birefringence hysteresis of a Boger fluid [Doyle *et al.* (1998)].

The short length scale behavior of individual molecules must be examined to understand the origins for the deficiencies of a coarse-grained model, such as the FENE dumbbell. Although the visualization techniques of Perkins *et al.* (1997) and Smith and Chu (1998) provide information about molecular conformations of individual molecules in an extensional flow, no existing experimental technique can measure intramolecular forces at the segmental level in an individual molecule subjected to extensional flow. Information about intramolecular forces along the backbone of a molecule is essential in order to predict accurately conformational changes in the molecule as well as the contribution of these forces to the total stress in the fluid. Since this information cannot be obtained experimentally, we obtain it through simulation of a fine-scale molecular model, the Kramers chain.

It is shown by Ghosh (2000) that the Kramers chain gives excellent agreement with the experimental observations for stress and birefringence in the start up of extensional flow up to Hencky strains of three to four. A direct comparison between experiments and the Kramers chain is not possible, because of the excessive computational expense involved in simulating Kramers chains of sufficient length to represent the molecules used in experiments. Instead, we show that for a given Weissenberg number, the stress in the Kramers chains of different lengths follows a universal curve until the chains approach their maximum extension. Longer chains follow this universal curve to larger strains before leveling off to a steady-state value. The universal curve gives excellent agreement with the experiments, particularly at low strains. A universal curve also was found for the transient birefringence growth for Kramers chains, and this also agreed well with the experimental data. Doyle and Shaqfeh (1998) also have shown that the evolution of molecular conformations of individual Kramers chains agrees well with observations of individual DNA molecules made by Perkins *et al.* (1997), Smith and Chu (1998), and Larson *et al.* (1999). They demonstrated that Kramers chains exhibit the same rich array of internal configurations (kinks, dumbbells, half-dumbbells, etc.) as real polymer molecules. The investigations referenced above suggest that the Kramers chain accurately describes the internal dynamics and internal forces within a polymer molecule. Hence, Brownian dynamics simulations of Kramers chains are used here to explore the reasons for the inadequacies of FENE dumbbells.

Previous efforts to understand the inadequacies of dumbbell models have resulted in conclusions that are not consistent with our findings. The existing literature is discussed here, and differences are highlighted with our conclusions in later sections. Rallison and Hinch (1988), Hinch (1994), and Rallison (1996) have tried to reconcile the differences between a Kramers chain and a dumbbell model by using the concept of a dissipative stress. They postulate that dissipative stress is an additional contribution to the stress tensor that is proportional to the rate-of-strain tensor and, therefore, drops instantaneously to zero when the rate of strain suddenly becomes zero. However, recent work by Rallison (1996) and Doyle *et al.* (1997) has shown that purely dissipative stresses are exhibited only by very short Kramers chains that are stretched at unrealistically high bead Peclet numbers. For longer chains, under more realistic flow conditions, the rapid stress growth simply results from the saturation of very short length scale elastic modes. Rallison (1996) recognized that elasticity acting on short enough length scales could have a very similar appearance to a dissipative stress. Hence, the modified dumbbell models of Hinch (1994) and Rallison (1996) contain dissipative stress terms in an attempt to approximate short length scale elasticity in a simple way. Their models possess an evolution equation for the distribution function that is the same as that for the FENE-P dumbbell model, but the polymer contribution to the stress consists of an elastic contribution, which is Hookean, and a dissipative contribution of the form $(\boldsymbol{\kappa}:\langle\mathbf{QQ}\rangle)\langle\mathbf{QQ}\rangle$. Here, $\mathbf{Q}$ is the end-to-end vector of a spring that has a maximum extensibility of $\mathbf{Q}_0$, and $\boldsymbol{\kappa}$ is the transpose of the velocity gradient tensor. In this formulation, the stress tensor is inconsistent with the standard Kramers expression containing the spring force for the dumbbell [Bird *et al.* (1987)]. An unphysical consequence of this dissipative stress is that it leads to stress jumps in the polymer contribution to the stress during instantaneous inception and cessation of flow; of course, such discontinuities are already present in the total stress due to the solvent contribution to the stress.

Verhoef *et al.* (1999) present a model that is closely related to the Hinch and Rallison models. The connector force of the dumbbell consists of a term that is a function of $\mathbf{Q}$ and a dissipative force term similar to that in the Hinch model. The model is more consistent with kinetic theory, because the dissipative stress is related directly to a component of the connector force. As a result, both the evolution equation for the conformation tensor and the equation for the stress tensor possess a dissipative term. Interestingly, this model results in a spring force that is not a simple function of the end-to-end distance but is also an explicit function of strain rate. In Sec. III, we present Brownian dynamics simulations that imply that the dumbbell connector force indeed varies with deformation history but its response is even more complex than that suggested by the Verhoef model. Although finite extensibility is not explicitly introduced through a Warner spring, finite extensibility results from the interaction of the two components of the force law. Consequently, the model is capable of accurately modeling steady-state behavior as well as transient stress growth. However, like the Hinch and Rallison models, the Verhoef model predicts a stress jump, in addition to the solvent contribution, upon instantaneous inception or cessation of extension. Although these models can approximate experimental data for stress growth in the start up of elongational flow, it should be remembered that they all contain at least one adjustable parameter that is not directly set by the physical model.

In addition to the prediction of stress, it is also important for a molecular model to capture the conformational changes of the molecules. In applications such as fiber spinning, film formation, and the production and film coating of pressure-sensitive adhesives, the chain conformation critically influences the material properties. Important information about molecular conformation also is obtained from measurements of birefringence. Doyle *et al.* (1998) adapted the filament stretching rheometer to measure birefringence,

and they were able to study directly the relationship of structure to stress of polymer solutions undergoing uniaxial elongational flow. By plotting stress versus birefringence, these researchers demonstrated the breakdown of the stress optical law in situations where the molecules become appreciably extended. Similar observations have been made by Li *et al.* (2000). Doyle showed that the breakdown of the stress-optical law was predicted by Kramers chains and by bead-spring models with nonlinear, finitely extensible springs (e.g., FENE dumbbells, FENE-P dumbbells, and FENE-P and FENE-PM chains). Doyle *et al.* also noticed that the stress–birefringence diagram for relaxation of fully stretched Kramers chains or finitely extensible bead-spring models is a universal curve.

A striking hysteretic behavior is observed when the extension and relaxation phases of the filament stretching experiment are considered together. Although all the above models predict the same universal relaxation curve, only the FENE dumbbell and Kramers chain display hysteresis. In contrast, Doyle *et al.* (1998) and Sizaire *et al.* (1999) demonstrated that the FENE-P dumbbell and the FENE-PM chain do not show hysteresis. We explain why some bead-spring models capture hysteresis whereas others do not. In addition, the paper provides a detailed understanding of the dynamics of polymer chains in the start up of elongational flow and of the mechanisms that lead to stress–birefringence hysteresis. This understanding will be helpful in constructing and evaluating new molecular models.

Sizaire *et al.* (1999) already have made some progress in understanding stress–birefringence hysteresis in dumbbell models. They put forward the hypothesis that hysteresis is always the result of coupled ''nonlinearity and dispersity;'' the force–extension relationship for the dumbbell must be nonlinear, and the distribution function must have dispersity (i.e., not be a delta function). For example, the FENE-P constitutive equation can be derived in two ways. First, the closure approximation may be interpreted as imposing a Gaussian form on the distribution function. In this case, the FENE-P spring force is linear in the end-to-end vector $\mathbf{Q}$. However, the FENE-P dumbbell is distinguished from the Hookean dumbbell, another model with a Gaussian distribution and a spring force linear in the end-to-end vector $\mathbf{Q}$, because the FENE-P spring force includes a denominator that is a function of the trace of the configuration tensor $\langle \mathbf{QQ} \rangle$. In this view the model has dispersity but not nonlinearity. Second, if the distribution function is assumed to be a delta function, then the FENE-P spring force is nonlinear in Q. This is because the trace of the configuration tensor $\langle \mathbf{QQ} \rangle$, which appears in the denominator of the FENE-P force law, is simply equal to the square of the extension of the molecules for a delta-function distribution function. With this approach, the FENE-P dumbbell model has nonlinearity but not dispersity. The FENE-P dumbbell model can have these two different interpretations, because the Peterlin closure approximation ensures that the evolution equation of the model depends only on $\langle \mathbf{QQ} \rangle$. Since two different distribution functions can have the same second moment, the FENE-P constitutive equation can be derived by assuming a distribution function that is either Gaussian or a delta function. However, the FENE-P dumbbell model never can be interpreted to have both nonlinearity and dispersity; and, hence, it does not predict hysteresis.

Lielens *et al.* (1999) further show that closure approximations of the FENE dumbbell model that assume disperse distribution functions and nonlinearity *do* predict hysteresis. They propose a FENE-L model that approximates the distribution function as a composite of a delta function and a rectangular segment. The addition of the rectangular segment adds dispersity to the distribution function. According to this picture, hysteresis in dumbbell models based on the Warner spring arises because the distribution function evolves through a different set of profiles during extension and relaxation. The birefringence is

only related to the second moment of the configuration tensor $\langle \mathbf{QQ} \rangle$, whereas the stress depends on other moments as well. Thus, during extension and relaxation distribution functions can assume different shapes that possess the same second moment, but do not predict the same stress. Therefore, hysteresis is possible in these formulations.

The model developed by Verhoef with a Peterlin closure approximation is an exception to the above framework of nonlinearity and dispersity as prerequisites for hysteresis. Before the closure approximation is applied, the spring force in the Verhoef dumbbell model is given by $Hh(Q^2)\mathbf{Q}+K(\boldsymbol{\kappa}:\mathbf{QQ})\mathbf{Q}$, where H scales the spring modulus, h is a linear function of Q^2, and the coefficient K is also constant. Following a Peterlin closure approximation, the spring force is given by $H\langle Q^2\rangle\mathbf{Q}+K(\boldsymbol{\kappa}:\langle \mathbf{QQ}\rangle)\mathbf{Q}$; and the distribution function for the end-to-end distance is a delta function. The model is neither nonlinear in $\mathbf{Q}$, nor does it possess dispersity. Nevertheless, it predicts hysteresis because, *unlike* the FENE models considered previously, the Verhoef model possesses a connector force with a term that depends on the strain history. During extension, the dissipative component of the end-to-end force law is nonzero and depends on the strain history through $\langle \mathbf{QQ} \rangle$. In contrast, the dissipative component of the spring force expression is always zero during relaxation. Therefore, hysteresis arises in the Verhoef model because the end-to-end force law is different during extension and relaxation. However, the shape of the hysteresis curve predicted by the Verhoef model differs from those of the FENE dumbbell or Kramers chain in one important way. Since there is a stress jump in the polymer contribution to the stress for the Verhoef model when the flow is turned off, the relaxation response begins with a vertical segment that is proportional in magnitude to the strain rate immediately prior to the cessation of the flow. Thus, as the strain rate is increased, the relaxation arm of the hysteresis curve does not tend to the universal curve observed by Doyle *et al.* (1998).

The Verhoef model belongs to a class of models with connector forces that depend on the current strain rate as well as the current end-to-end vector $\mathbf{Q}$. Another example is the Hookean dumbbell model with internal viscosity. The internal viscosity in this model is described by an extra term in the equation for the connector force, which is proportional to the rate of change of the end-to-end vector. Since the rate of change of the end-to-end vector is different during extension and relaxation, the Hookean dumbbell model with internal viscosity will display hysteresis. This is seen more easily by considering the expression for the stress tensor. Schieber and Öttinger (1994) demonstrated that inclusion of internal viscosity leads to an extra term in the stress tensor that is proportional to the velocity gradient tensor. Hence, the Hookean dumbbell with internal viscosity will display hysteresis because when the extension is stopped, there will be a stress jump and the relaxation arm of the hysteresis curve will be vertically displaced from the extension arm.

Neither the concept of a dissipative stress, as in the Verhoef model, nor the concept of internal viscosity, has rigorously been shown to be consistent with the physics embedded in finer grain models, such as the Kramers chain. In Sec. III, we show that the stress growth of a Kramers chain in an extensional flow is not consistent with an end-to-end force that depends only on the instantaneous strain rate. A more general model of the end-to-end connector force is required, one that depends on the entire deformation history. We will also show that the variation of the connector force with strain leads to a phenomenon that Doyle *et al.* (1998) referred to as ''configurational hysteresis.'' Configurational hysteresis is postulated to be an additional contribution to stress–birefringence hysteresis that is not captured by the evolution of the distribution function of the end-to-end distance. Instead, configurational hysteresis arises from configurational effects at a submolecular length scale that are not captured in current dumbbell models, such as the FENE dumbbell. For example, Kramers chain simulations show that the

molecules assume conformations with taut kinks or midsections during elongation, whereas they are crinkled and bear less stress for a given end-to-end distance during relaxation. In the previous work by Doyle *et al.* (1998), neither a method to quantify the magnitude of the configurational hysteresis nor a way to distinguish it from the hysteresis in the distribution function of the end-to-end distance was proposed. In Sec. V, we develop a method to achieve both of these objectives.

The shortcomings of dumbbell models have led several researchers to investigate multiple-mode alternatives. The FENE-P and FENE-PM chains show a more rapid stress growth than the FENE dumbbell at low strains due to the improved resolution of shorter time and length scales. As the number of modes is increased the transient stress growth at low strains better approximates a Kramers chain. Although multiple-mode models can always be relied upon to resolve shorter time-scale behavior, the addition of extra modes does not necessarily improve the description of hysteresis. For example, both the FENE-P and FENE-PM chains have been shown to predict the breakdown of the stress-optical rule, but only the FENE-P chain leads to hysteresis [Wiest (1998)].

Closure approximations can have a very important effect on finitely extensible bead-spring *chain* models. The FENE-P chain can be derived from the FENE chain model by assuming that the distribution functions for the end-to-end distances for each spring are separate delta functions whose evolutions are coupled due to the connectivity of the springs. Dispersity is introduced into the model by having several delta functions. Hysteresis arises because the *relative* behavior of these distribution functions is different during extension and relaxation. In contrast, the extra mode decoupling introduced in a FENE-PM chain model results in identical delta functions for the distribution functions of the end-to-end distance of each of the springs. Since dispersity has been removed from this model, it fails to predict hysteresis. Although several approximations to the FENE chain have been considered in the literature, the hysteresis of the FENE chain itself has not been investigated. In Sec. VI, we present a comparison of FENE chains with Kramers chains.

The paper is organized as follows. In Sec. II, various polymer models are discussed and the numerical techniques used to simulate their behavior are presented. The mechanisms that lead to stress growth during extension of Kramers chains and FENE dumbbells are explored in Sec. III. A comparison of the two models suggests ways in which dumbbell models should be modified in order to capture the finer scale dynamics of the Kramers chain. In Sec. IV, the relaxation behavior of the two models is described. Both models obey a universal relaxation curve during relaxation from fully stretched configurations. The more complex relaxation mechanisms that operate if relaxation begins from steady state or following an intermediate strain are explored. In Sec. V, the physical understanding of the extension and relaxation phases is combined to analyze hysteresis. A new method is presented to decouple configurational and distributional hysteresis and estimate the relative magnitude of each effect. Finally, the transient elongational rheological behavior and hysteresis of a FENE chain are examined in Sec. VI. It is shown that as more modes are added to a FENE chain, the agreement with the response of the corresponding Kramers chain improves.

II. POLYMER MODELS AND NUMERICAL SIMULATION TECHNIQUES

A. Freely draining Kramers chain model

The Kramers chain models a polymer molecule as N beads connected by $N-1$ rigid rods. The rods are each of length a, which corresponds to a Kuhn step [Flory (1953)]. The chains do not experience excluded volume interactions, i.e., the beads and rods can

move freely through one another. The rods rotate freely about the beads and are not subject to bending potentials. The solvent molecules are modeled as a continuum, which is described as an incompressible Newtonian liquid of viscosity η_s. This solvent imparts a deterministic Stokes law hydrodynamic drag and a stochastic Brownian force on each bead. The Stokes' drag on bead ν is proportional to the momentum space-averaged velocity of the bead relative to the solvent

$$\mathbf{F}_\nu^{(h)} = -\boldsymbol{\zeta}\cdot(\llbracket\dot{\mathbf{r}}_\nu\rrbracket - \mathbf{v}(\mathbf{r}_\nu,t)) \tag{1}$$

where $\mathbf{r}_\nu$ is the position of the νth bead, $\boldsymbol{\zeta}$ is the drag tensor, and $\mathbf{v}$ is the velocity of the incompressible Newtonian solvent. In this work, the drag is taken to be isotropic $\boldsymbol{\zeta} = \zeta\boldsymbol{\delta}$, and the scalar drag coefficient ζ is related to the bead radius ρ and solvent viscosity η_s, by

$$\zeta = 6\pi\eta_s\rho. \tag{2}$$

The Brownian-motion force due to the bombardment of the beads by the thermal motion of the solvent molecules is given by

$$\mathbf{F}_\nu^{(b)} = \sqrt{2kT}\mathbf{f}_\nu(t), \tag{3}$$

where $\mathbf{f}_\nu$ is a Gaussian white noise that is fully characterized by expressions for its mean and a two-time correlation function [Gardiner (1985)]:

$$\langle\mathbf{f}_\nu(t)\rangle = \mathbf{0}, \tag{4}$$

$$\langle\mathbf{f}_\nu(t)\mathbf{f}_\mu(t')\rangle = \delta_{\nu\mu}\boldsymbol{\delta}\delta(t-t'). \tag{5}$$

The presence of rigid rods requires that the equations of motion for the beads be solved subject to the constraint that the interbead separations remain constant. If we neglect the inertia of the beads, the equation of motion for bead ν reduces to

$$\mathbf{F}_\nu^{(h)} + \mathbf{F}_\nu^{(b)} + \mathbf{F}_\nu^{(c)} = \mathbf{0}, \tag{6}$$

where $\mathbf{F}_\nu^{(c)}$ is the constraint force arising from the tensions in the rods that are connected to bead ν. The constraint force is given by

$$\mathbf{F}_\nu^{(c)} = -\sum_{i=1}^{N-1}\gamma_i\frac{\partial}{\partial\mathbf{r}_\nu}\sigma_i, \tag{7}$$

where the $\{\gamma_i\}$ refer to $N-1$ undetermined Lagrange multipliers, and $\{\sigma_i\}$ are defined by

$$\sigma_i = (\mathbf{r}_{i+1}-\mathbf{r}_i)^2 - a^2 = 0. \tag{8}$$

If the flow field is homogeneous on the length scale of the polymer, then the solvent velocity may be rewritten as

$$\mathbf{v}(\mathbf{r}_\nu,t) = \mathbf{v}_0 + [\boldsymbol{\kappa}(t)\cdot\mathbf{r}_\nu(t)], \tag{9}$$

where $\mathbf{v}_0$ is the solvent velocity at the arbitrary fixed origin, and $\boldsymbol{\kappa}$ is the transpose of the velocity gradient tensor $\boldsymbol{\nabla}\mathbf{v}$. In this paper, we focus on transient elongational flows, for which the velocity field is given by

$$v_x = -\tfrac{1}{2}\dot{\epsilon}x, \quad v_y = -\tfrac{1}{2}\dot{\epsilon}y, \quad v_z = b\dot{\epsilon}z \tag{10}$$

where $\dot{\epsilon} = \dot{\epsilon}(t)$ is the time-dependent elongation rate. For the stress growth in a filament stretching experiment, $\dot{\epsilon}$ is a constant $\dot{\epsilon}_0$; and the Hencky strain ε is defined as $\dot{\epsilon}_0 t$. For the relaxation part of the experiment, $\dot{\epsilon}$ is zero. Since the fluid is assumed to be incom-

pressible, $\boldsymbol{\kappa}$ is traceless. Substituting Eq. (9) into Eq. (1) gives the Stratonovich-sense stochastic differential equations for the bead motions

$$\dot{\mathbf{r}}_\nu = \mathbf{v}_0 + [\boldsymbol{\kappa}\cdot\mathbf{r}_\nu] + \frac{1}{\zeta}\mathbf{F}_\nu^{(c)} + \frac{1}{\zeta}\mathbf{F}_\nu^{(b)}, \tag{11}$$

where the momentum-space-averaged bead velocity $[\![\dot{\mathbf{r}}_\nu]\!]$ is written simply as $\dot{\mathbf{r}}_\nu$.

The polymeric contribution to the stress tensor is calculated by using the Giesekus form of the stress tensor

$$\boldsymbol{\tau}_p = \tfrac{1}{2} n_p \zeta \sum_\nu \langle \mathbf{R}_\nu \mathbf{R}_\nu \rangle_{(1)}, \tag{12}$$

where n_p is the number density of polymer molecules and $\mathbf{R}_\nu$ is the position of bead ν with respect to the center of mass of the molecule. The angled brackets $\langle\,\rangle$ represent an average with respect to the configurational distribution function, and the subscript (1) denotes the upper convected derivative.

The end-to-end vector of the molecule is important for understanding the configurational behavior of the polymer molecule. In terms of the bead vectors for the Kramers chain, the end-to-end vector is defined as $\mathbf{Q} = \mathbf{r}_N - \mathbf{r}_1$. The end-to-end length of the molecule is given by the magnitude of $\mathbf{Q}$.

For analysis of stress–birefringence hysteresis, the birefringence of a polymer solution extended in the z direction is calculated from the expression used by Doyle (1997):

$$\Delta n = n_{zz} - n_{xx} = 5 C n_p kT \sum_{\nu=1}^{N-1} \langle u_{\nu z} u_{\nu z} - u_{\nu x} u_{\nu x} \rangle, \tag{13}$$

where

$$C = \frac{2\pi}{45kT}\frac{(n^2+2)^2}{n}(\alpha_1 - \alpha_2).$$

$n = \frac{1}{3}\operatorname{tr}\mathbf{n}$ is the isotropic part of the refractive index tensor, α_1 and α_2 are the polarizabilities parallel and perpendicular to a rod, respectively, and $u_{\nu x}$ and $u_{\nu z}$ are the x and z components of the unit vector in the direction of the connector vector $(\mathbf{r}_{\nu+1} - \mathbf{r}_\nu)$.

It remains to define the appropriate dimensionless groups used in the simulations. The characteristic quantities used to nondimensionalize the equations are the characteristic length a, the characteristic diffusive time for an individual rod, $\lambda_R = \zeta a^2/kT$, and the characteristic Brownian force, kT/a. The bead Peclet number is defined as the product of the time constant of an individual rod multiplied by the extension rate

$$\mathrm{Pe} \equiv \frac{\zeta a^2}{kT}\dot{\epsilon}_0 = \lambda_R \dot{\epsilon}_0. \tag{14}$$

From simulations of Kramers chains in relaxation following the cessation of shear flow, Doyle *et al.* (1997) found that the longest time scale, λ_d, of the polymer is related to the time constant of a rod by

$$\lambda_d = 0.0142\, N^2 \frac{\zeta a^2}{kT}. \tag{15}$$

The Weissenberg number is defined as λ_d multiplied by the extension rate. Hence, by combining Eqs. (14) and (15), the Weissenberg number is related to the rod Peclet number by

$$\mathrm{Wi} \equiv 0.0142\, N^2\, \mathrm{Pe}. \tag{16}$$

It would take a Kramers chain of approximately 2850 rods to represent the polystyrene Boger fluid of $M_w = 2.25\times 10^6$ g/mol used by Spiegelberg *et al.* [Ghosh (2000); Chap. 7]. Due to limits on computational resources, chains of this length cannot presently be simulated. The simulations in this study were conducted with chains of 40 rods in order to test whether the Kramers chain model could qualitatively capture the experimental observations. We use the iterative scheme developed by Liu (1989) to integrate the stochastic differential equations [Eq. (11)] subject to the constraints. The dimensionless time step is taken to be 1.0×10^{-5} in the simulations and the constraints are satisfied to a relative tolerance of 1.0×10^{-6}.

B. Bead-spring models

Bead-spring models are coarse-grained versions of the Kramers chain in which the entropic elasticity of subsections of the chain are represented by springs. Assuming no bead inertia, we write the balance between hydrodynamic, Brownian, and spring forces ($\mathbf{F}_\nu^{(s)}$) on bead ν as

$$\mathbf{F}_\nu^{(h)} + \mathbf{F}_\nu^{(b)} + \mathbf{F}_\nu^{(s)} = \mathbf{0}. \tag{17}$$

The Brownian and hydrodynamic forces have the same form as for the Kramers chain. Therefore, Brownian dynamics simulations of these models can be readily performed without the complications of imposing constraints, as described by Öttinger (1996). Information about the configurational distribution function can then be built up from an ensemble of Brownian trajectories. The evolution of the distribution function also can be predicted by solving the equivalent Fokker–Planck equation for the bead-spring models:

$$\frac{\partial \psi}{\partial t} = -\sum_{j=1}^{M} \frac{\partial}{\partial \mathbf{Q}_j} \cdot \left\{ [\boldsymbol{\kappa}\cdot\mathbf{Q}_j]\psi - \frac{1}{\zeta} \sum_{k=1}^{M} A_{jk} \left[kT \frac{\partial}{\partial \mathbf{Q}_k} \psi + \mathbf{F}_k^{(s)} \psi \right] \right\}, \tag{18}$$

where $\psi(\mathbf{Q}^M, t)$ is the probability of finding a chain with the set of spring vectors $\{\mathbf{Q}^M = \mathbf{Q}_1, \mathbf{Q}_2, \ldots, \mathbf{Q}_M\}$ at time t, M is the number of springs, and A_{jk} is the Rouse matrix as defined in Bird *et al.* (1987). Although, a formal mathematical equivalence exists between the Brownian dynamics and Fokker–Planck formulations, it is easier to see how the spring force affects the evolution of the distribution function in the Fokker–Planck formulation.

The spring force is also required in the calculation of the stress. The stress tensor for a bead-spring model is given by the Kramers expression

$$\tau_p = M n_p kT \boldsymbol{\delta} - n_p \sum_{i=1}^{M} \langle \mathbf{Q}_i \mathbf{F}_i^{(s)} \rangle. \tag{19}$$

The birefringence of bead-spring models is calculated by using the expression in Eq. (20), which is taken from Wiest (1998), as

$$\Delta n = 5C n_p kT \frac{n_s}{Q_0^2} \sum_{i=1}^{M} \langle Q_{iz} Q_{iz} - Q_{ix} Q_{ix} \rangle, \tag{20}$$

where Q_0 is the maximum extension of a spring and each spring corresponds to n_s rods in the Kramers chain representation of the polymer. A similar expression is also used by Li and Larson (2000). The remainder of this section focuses on the origin and the form of the spring force for these models.

C. FENE dumbbell

The FENE dumbbell model consists of two beads connected by an elastic spring. The spring force is directed along the vector **Q** connecting the two beads; and the magnitude of the force is a function of the bead separation. For small extensions, the spring force is linear in the bead separation. The proportionality constant H_d is related to the parameters of the Kramers chain by

$$H_d = \frac{3kT}{(N-1)a^2}. \tag{21}$$

For larger extensions, the force law becomes nonlinear, and Flory (1953) has shown that the force required to hold the ends of the chain at a fixed separation is given by the inverse Langevin function. An approximation to this function, which is computationally more tractable, was developed by Warner and is referred to as the FENE force law. The FENE force law is given by

$$F^{(s)}(Q) = \frac{H_d Q}{(1-Q^2/Q_{0d}^2)}, \tag{22}$$

where Q_{0d} is the maximum extension of the dumbbell and is given by

$$Q_{0d} = (N-1)a. \tag{23}$$

The maximum extension of the spring is often expressed by the dimensionless parameter b, which is defined as

$$b \equiv \frac{H_d Q_{0d}^2}{kT}. \tag{24}$$

Substituting Eqs. (21) and (23) into Eq. (24) yields

$$b = 3(N-1). \tag{25}$$

The inverse Langevin force law (and the FENE approximation to it) is obtained from equilibrium statistical mechanics and is based on the assumption that for a given end-to-end distance a Kramers chain has had sufficient time to sample its entire configuration space and that the internal conformational distribution function has reached equilibrium. This force law should be used with caution in nonequilibrium situations. Only when the time scale of the deformation is much longer than the relaxation time scale of the entire chain will the chain unravel *reversibly*, i.e., the internal conformation distribution of the chain will be able to equilibrate at each stage of the stretching. Smith and Chu (1998) have shown that during the nonergodic dynamics of a rapid elongation, kinked conformations are very common; however, these conformations are very uncommon in slow flows. These observations provide a micromechanical basis for anticipating that the FENE force law will not be applicable under rapid stretching conditions. This is indeed seen in Sec. III, where the reversible stretching condition is shown to be violated in a strong extensional flow and the FENE force law is shown no longer to be applicable.

The time constant λ_d for a FENE dumbbell is $\zeta_d/4H_d$ so that the Weissenberg number is

$$\mathrm{Wi} = \lambda_d \dot{\epsilon} = \frac{\zeta_d \dot{\epsilon}}{4H_d}, \tag{26}$$

where ζ_d is the drag coefficient of a bead in the FENE dumbbell model. By combining Eqs. (15) and (21), ζ_d is related to the drag coefficient on a bead in a Kramers chain as

$$\zeta_d = 0.1704 \frac{N^2}{N-1} \zeta. \tag{27}$$

D. FENE chain

A FENE chain models a polymer molecule as a set of beads connected by FENE springs. We begin with a molecule of a given time constant λ_d and discretize it into a chain with an increasing number of sections. An individual spring now represents a short section of the Kramers chain instead of the chain as a whole. For M springs, the maximum extension of each spring is $[(N-1)/M]a$, and the spring constant of an individual spring is

$$H_s = \frac{3MkT}{(N-1)a^2}. \tag{28}$$

As M increases and each spring represents a shorter fragment of the molecule, each spring becomes stiffer.

The time constant λ_s for an individual spring is $\zeta_s/4H_s$. In order to relate this time constant to the time constant of a FENE dumbbell that represents the same molecule, a scaling relationship must be developed between ζ_s and ζ_d. The scaling relationship is chosen so that the transient extensional viscosity of the FENE chains approaches the profile predicted by the Kramers chain as M becomes large. We show in Sec. VII that this condition can be satisfied by a scaling relationship that makes the zero-shear-rate first normal stress coefficient independent of M. Using the result for the zero-shear-rate first normal stress coefficient presented by Wiest and Tanner (1989) gives the relationship between ζ_d and ζ_s as

$$\lambda_s = \frac{\zeta_s}{4H_s} = \frac{((b_s+5)/b_s)(b_d/\sqrt{(b_d+5)(b_d+7)})(\zeta_d/4H_d)}{\left\{\frac{(2(M+1)^2+7)((M+1)^2-1)}{45} - \frac{12((M+1)^2+1)((M+1)^2-1)}{45(M+1)(b_s+7)}\right\}^{1/2}}, \tag{29}$$

where the parameter b_s in Eq. (29) is the finite extensibility parameter of an individual spring in the FENE chain. Since each spring now represents a section of the Kramers chain, b_s is proportional to the number of rods allocated to each section of the Kramers chain and is related to N and M by

$$b_s = \frac{3(N-1)}{M}. \tag{30}$$

Other scaling relationships do not satisfy condition (29) mentioned above. In particular, a scaling relationship that makes the zero-shear-rate viscosity independent of M results in

TABLE I. Simulation parameters.

Simulation No.	N_{Kramers}	Wi	Maximum strain	Kramers ensemble	b (FENE)	FENE ensemble
1	25	11.4	5	25 000	⋯	
2	41	11.4	5	25 000	120	100 000
3	63	11.4	5	15 000	⋯	
4	41	4.5	5	15 000	⋯	
5	41	11.4	2.5	25 000	120	100 000

an expression for the steady-state extensional viscosity of the FENE chains that deviates from the Kramers chain prediction for $M \gg 1$.

For the FENE force law to hold for the individual springs, the time scale of the deformation must be much longer than the relaxation time of a section. Since the time constant of an individual spring scales with M^{-2}, for chains consisting of 10–20 identical springs, strain rates needed to violate this condition cannot be physically realized. Thus, we expect the transient extensional behavior and hysteretic properties of FENE chains to be in better agreement with Kramers chain predictions than those for FENE dumbbells. This expectation will be confirmed in Sec. VII. The Brownian dynamics algorithm used to simulate the FENE chains and the FENE dumbbell was identical to that of van den Brule (1993).

III. UNIAXIAL EXTENSIONAL FLOW

In the kinetic theory of bead-spring polymer models, the spring force law appears in two places: in the evolution equation for the distribution function [Eq. (18)] as the intramolecular force and in the equation for the stress tensor [Eq. (19)]. In this section the evolution of the end-to-end distribution function and the end-to-end force are compared for a Kramers chain and an equivalent FENE dumbbell. A FENE dumbbell model is a coarse-grained approximation to a Kramers chain under the reversible stretching conditions described in Sec. II. In extensional flows at large strain rates, however, Kramers chains are stretched out very rapidly; and the reversible stretching condition is not satisfied. We show that the violation of the reversible stretching condition leads to a deviation of the FENE force law from the effective ensemble-averaged end-to-end force in the Kramers chain. We then consider the implications of a modification to the FENE force law in Eqs. (18) and (19) for the prediction of transient stress growth.

Table I shows the simulations that were conducted in order to compare Kramers chains and FENE dumbbells. Simulations (1)–(3) were conducted at Wi = 11.4 for Kramers chains of 24, 40, and 62 rods in order to assess the effects of chain length. Simulations (4) and (5) examine the effects of varying Wi for a chain of 40 rods. Simulations (2) and (5) were also performed for an equivalent FENE dumbbell at the same Wi.

The growth of stress, birefringence, and root-mean-square end-to-end distance, $\langle Q^2 \rangle^{1/2}$, with Hencky strain in start up of elongational flow are compared in Figs. 1–3. As noted by Doyle *et al.* (1998), the Kramers chain and the FENE dumbbell predict the same steady-state values for stress and birefringence; however, the Kramers chain predicts faster growth of these properties at low strains than does the FENE dumbbell model. Both transient stress and birefringence depend upon the configuration of the entire molecule. Therefore, it is not surprising that the Kramers chain, which has many shorter length scale (and, therefore, shorter time scale) modes available to it, responds more

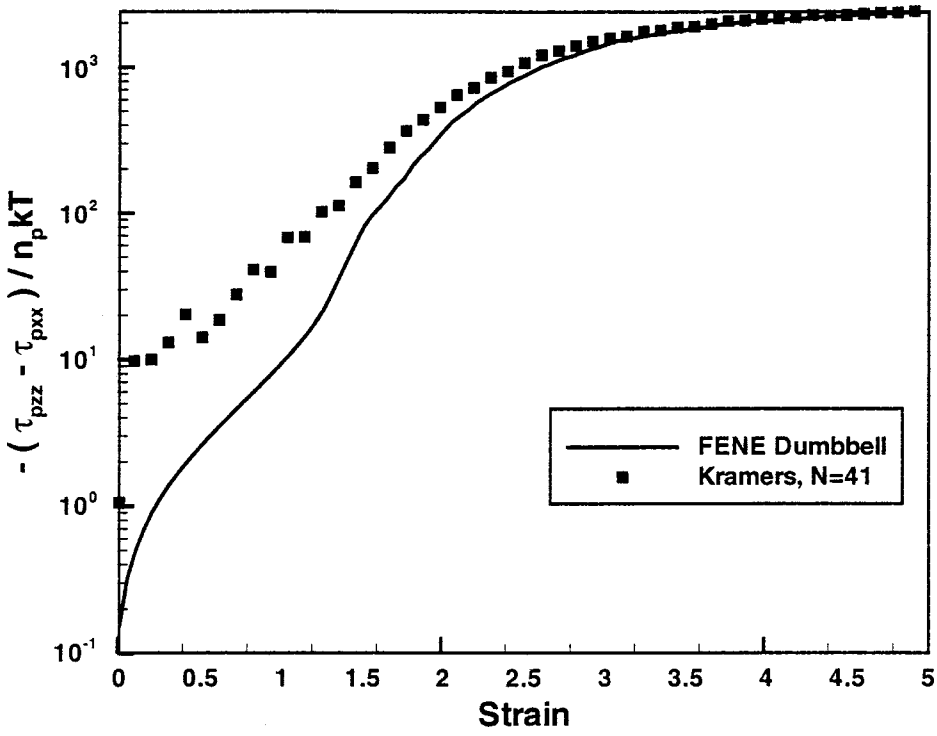

FIG. 1. Dependence of stress on strain for $N = 41$ Kramers chains and equivalent FENE dumbbells in uniaxial extension at Wi = 11.4.

quickly to the inception of extensional flow. In contrast, the overall size of the polymer molecule, $\langle Q^2 \rangle^{1/2}$, evolves more slowly for the Kramers chain than for the FENE dumbbell. This is because a dumbbell model can only stretch through an increase in Q. In contrast, a Kramers chain can stretch without the ends being pulled apart. It seems, therefore, that the end-to-end distance may not be the most meaningful measure of conformation for Kramers chains in transient extensional flow. Nevertheless, in this paper we use Q as the measure of the conformation of an entire Kramers chain because we wish to compare the end-to-end force in Kramers chains with that in FENE dumbbells for which the entropic spring force is defined strictly in terms of Q.

In order to compare the response of the end-to-end distance of the molecules as described by the FENE dumbbell and Kramers chain models, we construct two contracted distribution functions which give the probability of finding a molecule with a specific end-to-end distance Q. For the FENE dumbbell, the distribution function for the end-to-end distance is the following contraction of $\psi(\mathbf{Q},t)$:

$$\psi(Q,t) = \int\int \psi(Q,\theta,\phi,t) d\theta d\phi, \tag{31}$$

where Q, θ, and ϕ are the length and spherical polar angles describing the end-to-end vector $\mathbf{Q}$. We define $\psi_K(Q,t)$ as the contraction of the full configurational distribution function of the Kramers chain over the end-to-end distance:

$$\psi_k(Q,t) = \int \psi_{\text{Kramers}}(\mathbf{x},t)\, \delta\left(Q - \left| a \sum_{i=1}^{N-1} \mathbf{u}_i \right| \right) d\mathbf{x}. \tag{32}$$

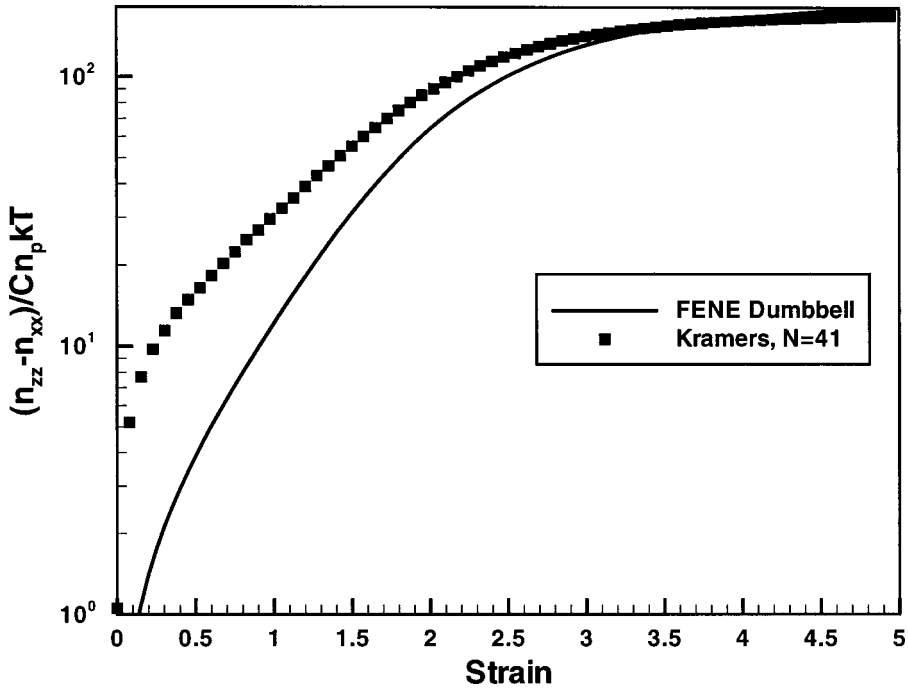

FIG. 2. Dependence of birefringence on strain for $N = 41$ Kramers chains and equivalent FENE dumbbells in uniaxial extension at Wi = 11.4.

Thus, ψ_K gives that fraction of Kramers chains that have end-to-end distance Q, independent of the detailed internal configuration.

The contracted distribution function $\psi_K(Q,t)$ is determined from Brownian dynamics simulations of an ensemble of Kramers chains by calculating the fraction of molecules with a specified end-to-end distance. The evolution of $\psi_K(Q,t)$ for a Kramers chain of 41 beads and $\psi(Q,t)$ for the equivalent FENE dumbbell [simulation (2)] during start up of uniaxial extension are compared in Figs. 4 and 5. The shapes of the distribution functions over the entire domain of Q are shown in Fig. 4 up to $\epsilon = 1.5$. The peak that forms near the maximum extension for strains between 2.5 and 5 is the focus of Fig. 5. Both the FENE dumbbell and Kramers chain models exhibit qualitatively similar behavior. At low strains, the peak of the distribution function gradually migrates from its equilibrium value to higher extensions with increasing strain (see Fig. 4); the tail of the distribution function for large Q broadens out and eventually reaches the maximum extension. Once the tail has reached maximum extension, a peak begins to form near Q_0. At $\epsilon = 1.5$, the peak near maximum extension is already very prominent for the FENE dumbbell, whereas it is not yet clearly distinguished for the Kramers chain. An exchange of probability density then ensues between the peaks at low extension and high extension. The shapes of the end-to-end distribution functions for the two models for strains between 2.5 and 5 are illustrated in Fig. 5. At $\epsilon = 2.5$, $\psi(Q,t)$ for the FENE dumbbell is close to its final steady-state shape; however, the peak in $\psi_K(Q,t)$ for the Kramers chain has only grown to 25% of its final height. The maximum in the peak at $\epsilon = 5$ is located at a slightly higher value of Q for the Kramers chain; this peak is also broader than the peak for the FENE dumbbell, but is only half the height. Keunings (1997) also investigated the evo-

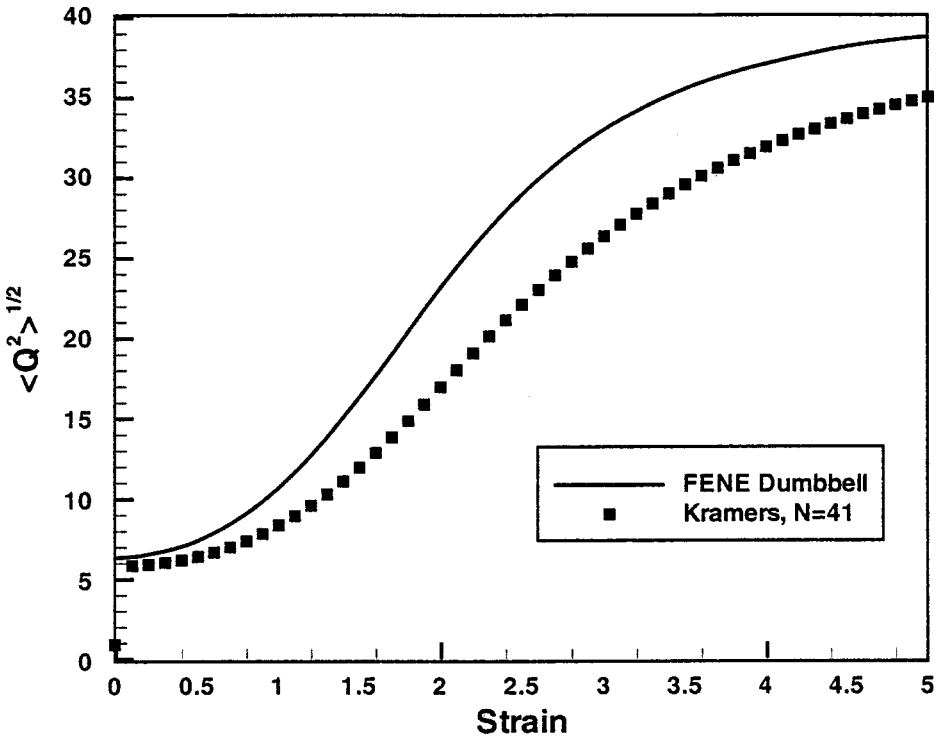

FIG. 3. Dependence of $\langle Q^2\rangle^{1/2}$ on strain for $N = 41$ Kramers chains and equivalent FENE dumbbells in uniaxial extension at Wi = 11.4.

lution of the distribution function of a FENE dumbbell in uniaxial extensional flow. His observations are in agreement with the results for the FENE dumbbell presented here.

The most noticeable difference between the evolutions of the end-to-end distribution functions for the two models is that $\psi(Q,t)$ of the FENE dumbbell shifts to larger extensions much more quickly than $\psi_K(Q,t)$ for the Kramers chain. This can be seen in the larger peak near maximum extension at $\epsilon = 1.5$ for the FENE dumbbell in Fig. 4. Based on this observation, if the end-to-end force of the Kramers chain were well described by the FENE force law (as is assumed whenever the FENE dumbbell model is used as a rheological model), the stress growth predicted at low strains would be larger for the FENE dumbbell than the Kramers chain. However, the results in Fig. 1 show the opposite effect. This result suggests that the effective end-to-end force of the Kramers chain is poorly approximated by the FENE expression, at least under transient, rapid stretching conditions. In the rest of this section, we outline a procedure to estimate the ensemble-averaged end-to-end force profile for a Kramers chain, and we demonstrate that this result deviates markedly from the FENE force law in extensional flows.

For an ensemble of N_s dumbbells with an arbitrary force law $\mathbf{F}^{(s)}(\mathbf{Q},t)$ that is a function of $\mathbf{Q}$ and time only, the polymer contribution to the stress tensor is given by the Kramers form of the stress tensor [Bird *et al.* (1987)] as

$$\boldsymbol{\tau}_p(t) = n_p kT\boldsymbol{\delta} - \frac{n_p}{N_s}\sum_{n=1}^{N_s}\mathbf{Q}_n\mathbf{F}_n^{(s)}(\mathbf{Q}_n,t), \tag{33}$$

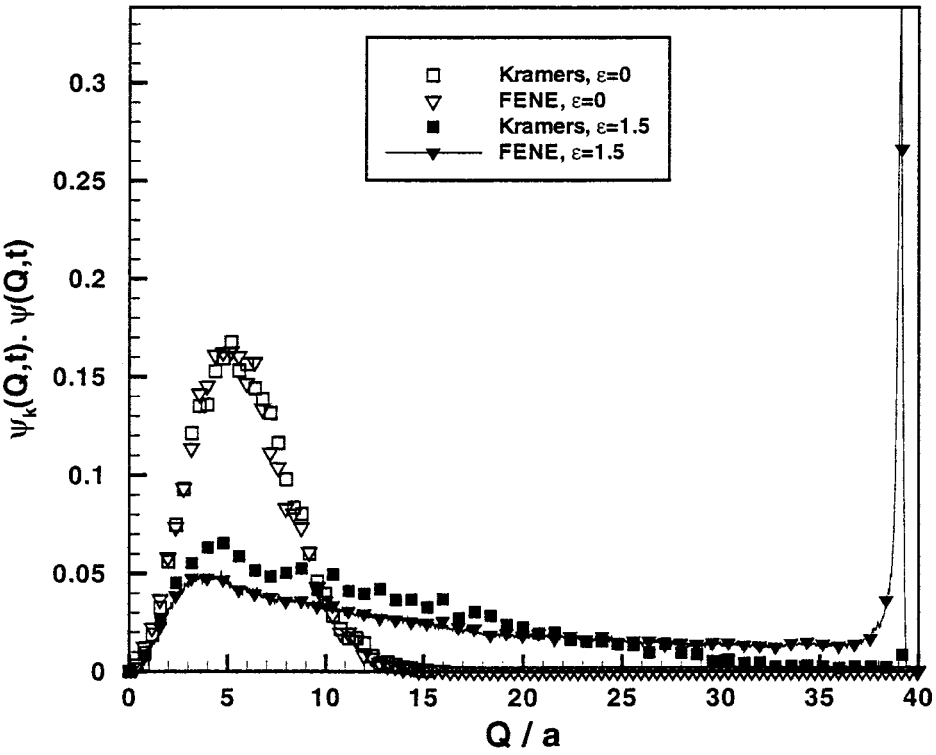

FIG. 4. Evolution of the end-to-end distribution function up to $\varepsilon = 1.5$ for $N = 41$ Kramers chains and equivalent FENE dumbbells in uniaxial extension at Wi = 11.4.

in which the ensemble average is expressed as a summation. The subset of N_Q molecules with end-to-end distances between Q and $Q+dQ$, will contribute to the zz component of the stress $\tau_{pzz,Q}$ approximately as

$$\tau_{pzz,Q} \approx n_p kT \frac{N_Q}{N_s} - n_p \frac{Q_z}{N_s} \sum_{n=1}^{N_Q} F_{zn}. \tag{34}$$

Since the summation is over all molecules with a given end-to-end distance Q, the z component of Q cannot strictly be factored out of the summation since not all molecules with a given end-to-end distance Q have the same Q_z. However, in a uniaxial elongation the approximation that $Q_z \approx Q$ is a good one, except for very small strains. In our simulations, effective forces are calculated for strains of unity or greater. For the lowest strain rates investigated, Q_z was already 95% of the overall end-to-end distance of the molecule at a strain of unity. As a result, in the rest of the paper, whenever an expression for force or stress containing Q is presented, it is implicitly assumed that the approximation $Q_z \approx Q$ was used during the calculations.

The contribution of the subset of N_Q molecules with end-to-end distances between Q and $Q+dQ$ to the zz component of the stress in an ensemble of Kramers chains can also be given by the Giesekus expression

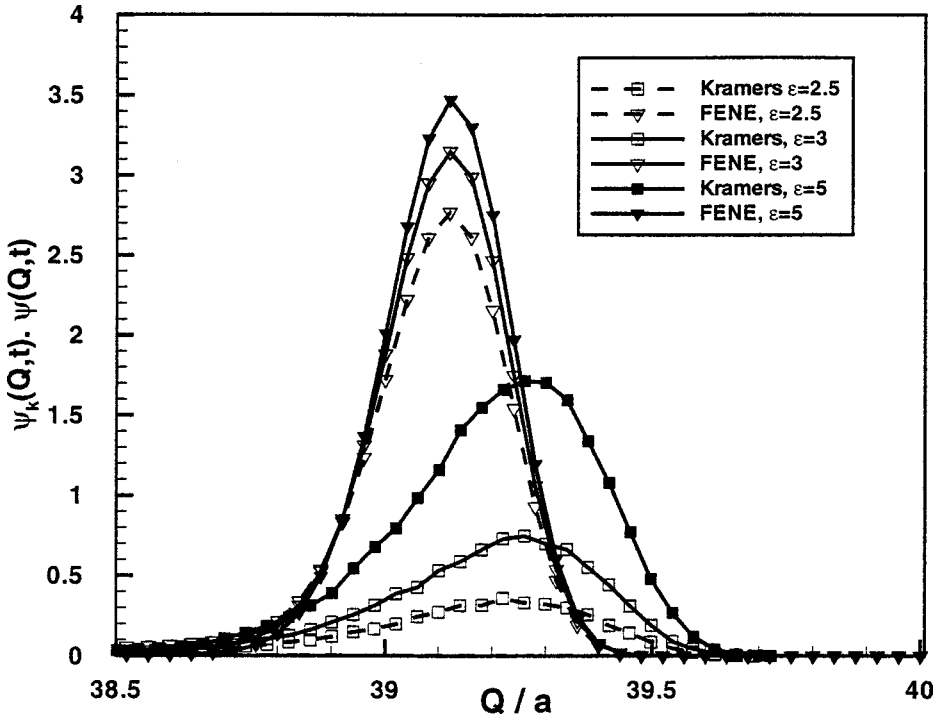

FIG. 5. Evolution of the end-to-end distribution function between strains of 2.5 and 5 for $N = 41$ Kramers chains and equivalent FENE dumbbells in uniaxial extension at Wi = 11.4.

$$\boldsymbol{\tau}_{pzz,Q} = \frac{1}{2}\frac{n_p\zeta}{N_s}\sum_{n=1}^{N_Q}\left\{\frac{d}{dt}\left(\sum_{\nu=1}^{N}\mathbf{R}_\nu\mathbf{R}_\nu\right)_n - \boldsymbol{\kappa}\cdot\left(\sum_{\nu=1}^{N}\mathbf{R}_\nu\mathbf{R}_\nu\right)_n - \left(\sum_{\nu=1}^{N}\mathbf{R}_\nu\mathbf{R}_\nu\right)\cdot\boldsymbol{\kappa}^\dagger\right\}_{zz}. \tag{35}$$

Equating Eqs. (34) and (35) gives the z component of the effective ensemble-averaged spring force in the Kramers chain $F_{z,\text{effective}}$ as

$$F_{z,\text{effective}}(Q,t) = \frac{1}{N_Q}\sum_{n=1}^{N_Q}F_{zn} = \frac{kT}{Q} - \frac{1}{2}\frac{\zeta}{N_Q Q}\sum_{n=1}^{N_Q}\left\{\frac{d}{dt}\left(\sum_{\nu=1}^{N}\mathbf{R}_\nu\mathbf{R}_\nu\right)_n - \boldsymbol{\kappa}\cdot\left(\sum_{\nu=1}^{N}\mathbf{R}_\nu\mathbf{R}_\nu\right)_n - \left(\sum_{\nu=1}^{N}\mathbf{R}_\nu\mathbf{R}_\nu\right)\cdot\boldsymbol{\kappa}^\dagger\right\}_{zz}. \tag{36}$$

If the end-to-end force of the Kramers chain were accurately described by the inverse Langevin function, $F_{z,\text{effective}}$ would equal the inverse Langevin function. In general, however, we find that $F_{z,\text{effective}}$ varies with end-to-end distance and time.

From the simulations, the effective force profile at a given strain is determined in the following way. The range of possible end-to-end distances of a Kramers chain $[0 \leqslant Q$

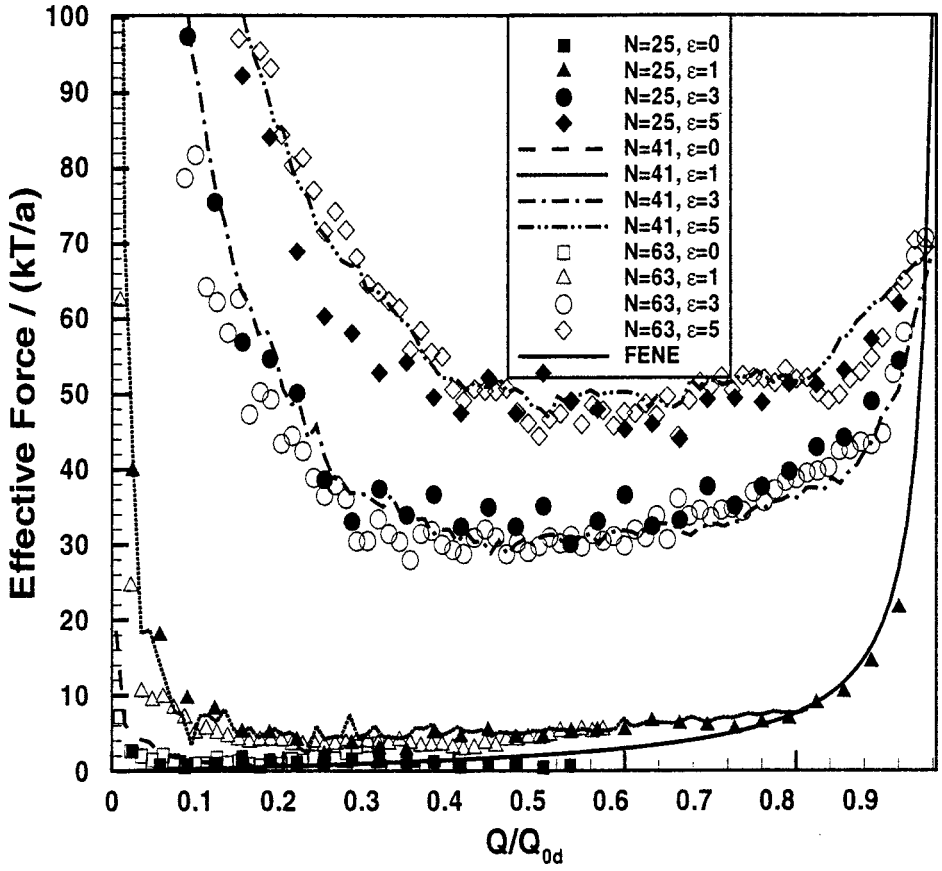

FIG. 6. Evolution of the effective end-to-end force profiles up to $\varepsilon = 5$ for $N = 41$ Kramers chains in uniaxial extension at Wi = 11.4.

$\leqslant (N-1)a]$ is divided into $25(N-1)$ bins of equal width $0.04a$. An ensemble of Kramers chains is frozen at a given strain, and the molecules are placed into bins according to their end-to-end distance. The effective force for the value of Q at the midpoint of a bin is calculated according to Eq. (36). Even with ensembles of 15 000 and higher, the number of molecules in some bins is not large enough to ensure a low error in the average value of the effective force. Therefore, molecules are collected in bins over 100 time steps instead of at a single time step. At Wi = 10, this is equivalent to a Hencky strain of 0.01 if the dimensionless time step is 1.0×10^{-5}. Time averaging introduces a small error, because the molecules in each bin do not all correspond to exactly the same strain. For intermediate strains, at moderate values of Q, there is approximately a 2% difference between the effective force at the beginning and end of the time interval. However, time averaging reduced the statistical error in the estimate of the mean effective force from 50% to 4%. Rallison (1996) used a similar noise reduction technique.

Effective force profiles constructed at various strains for simulations (1), (2), and (3) are shown in Fig. 6 with Wi = 11.4. The effective force is not a function of Q alone, but changes with strain. At equilibrium, the effective force profile agrees well with the FENE force law except for very small Q. The deviation for small Q at equilibrium is due to numerical error that arises when a small statistical error in the stress of the Kramers

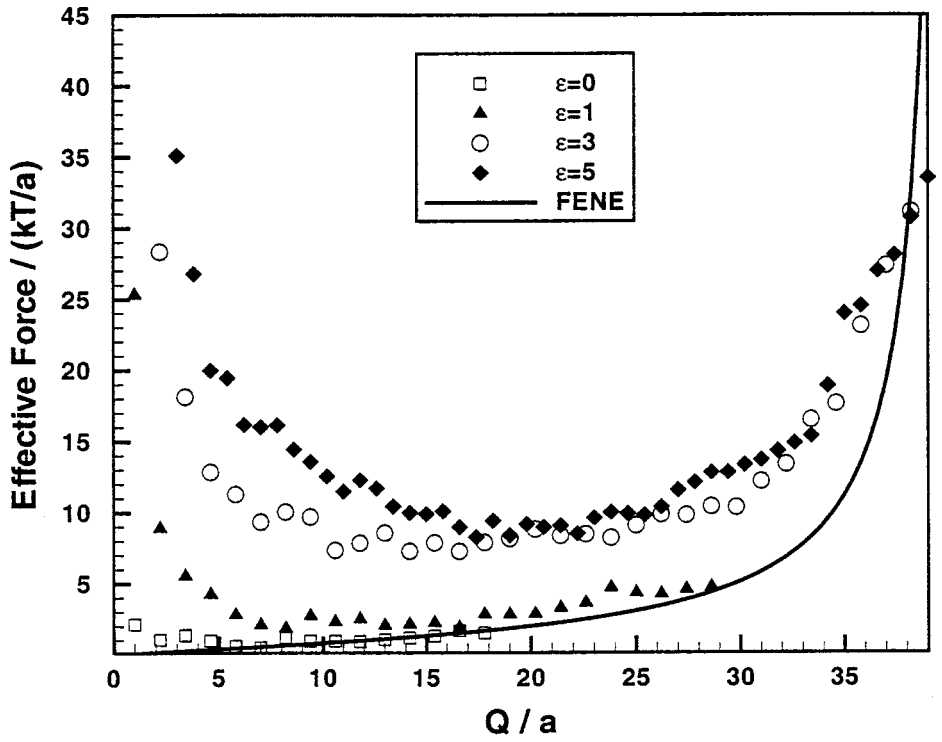

FIG. 7. Evolution of the effective end-to-end force profiles up to $\varepsilon = 5$ for $N = 41$ Kramers chains in uniaxial extension at Wi = 4.5.

chains is divided by a very small value of Q. In addition, part of the error may also be attributed to the fact that the approximation $Q_z \approx Q$ is used, and the end-to-end distance Q of a molecule is approximated by Q_z, which has a smaller value. For all nonzero strains, the effective force profiles lie above the FENE curve except near Q_0. Additionally, the force profiles move upwards with increasing strain. The upward movement of the entire force *profile* with increasing strain will be referred to in the rest of the paper as ''strain hardening'' of the effective end-to-end force. The results in Fig. 6 also demonstrate that, for a given strain, the force profile is independent of N for Kramers chains with $N > 25$. This suggests that the behavior of Kramers chains long enough to represent the high molecular weight Boger fluids typically used in filament-stretching experiments can be adequately probed by simulating much shorter chains.

It is not a numerical artifact that at nonzero strains, the effective force becomes unbounded as $Q \to 0$. A Kramers chain in a strongly extensional flow may make a large contribution to the fluid stress if it has unraveled a great deal and possesses a large number of kinks. However, its ends may be close to one another. In the equation for the effective force [Eq. (36)], the last term has a large numerator and a small denominator. Hence, the effective force is very large. The effective forces at low Q increase with strain, because the rest of the chain can unravel and contribute a larger stress to the fluid, even though the end points of a Kramers chain may remain close together.

The evolution of the effective force profiles for a 41-bead Kramers chain at Wi = 4.5 [simulation (4)] is shown in Fig. 7. The effective force profiles still move upwards with increasing strains, but to a much smaller extent than at Wi = 11.4. As the extension rate decreases, the deviation of the effective force from the FENE force de-

creases, because the system more nearly satisfies the reversible stretching condition. Hence, the FENE force law better approximates the end-to-end force law, as expected.

The effective forces shown in Figs. 6 and 7 are always better approximated by the FENE force law at larger Q. The convergence of the effective force and the FENE force occurs because the configuration space of the chain contracts as the chain is extended. Consequently, the chain can sample a larger portion of its configuration space at a given Q before it is stretched further. In the limit of full extension, the configuration space has shrunk so much that the chain can manage to sample it all, despite the presence of a strong underlying flow. Hence, the reversible stretching criterion is met in these extreme conditions, and the FENE force law is a good approximation of the end-to-end force in the Kramers chain.

The behavior of the effective force observed above indicates that the entire end-to-end force *profile* depends on both the strain and the strain rate for strong, transient extensional flows. Consequently, the end-to-end force profile has been shown to be dependent upon the deformation history, unlike the inverse Langevin or FENE force expressions.

Having demonstrated the deviation of the effective end-to-end force of the Kramers chain from the predictions of the FENE model, the impact of this deviation on the stress growth is now considered. The stress in the Kramers chain is split into a FENE and a non-FENE contribution. The FENE contribution to the stress is given by

$$\boldsymbol{\tau}_p^{\mathrm{FENE}} = n_p kT\boldsymbol{\delta} - n_p \int \mathbf{Q}^{\mathrm{Kramers}}\mathbf{F}^{\mathrm{FENE}}\psi_K(\mathbf{Q}^{\mathrm{Kramers}},t)\,d\mathbf{Q}^{\mathrm{Kramers}}, \tag{37}$$

where the ensemble average is taken with respect to $\psi_K(\mathbf{Q}^{\mathrm{Kramers}},t)$ of the Kramers chain, the end-to-end *vector*, $\mathbf{Q}^{\mathrm{Kramers}}$, is that of the Kramers chain, and the end-to-end force is assumed to be the FENE force evaluated for $\mathbf{Q}^{\mathrm{Kramers}}$. The contracted distribution function $\psi_K(\mathbf{Q}^{\mathrm{Kramers}},t)$ is defined similarly to Eq. (32). The *zz* component of this stress is given by

$$\boldsymbol{\tau}_{\mathrm{pzz}}^{\mathrm{FENE}} = n_p kT - n_p \int Q_z^{\mathrm{Kramers}} F_z^{\mathrm{FENE}}\psi_K(\mathbf{Q}^{\mathrm{Kramers}},t)\,d\mathbf{Q}^{\mathrm{Kramers}}. \tag{38}$$

The orientation of molecules along the stretching direction in a uniaxial elongational flow allows us to approximate this three-dimensional integral by a one-dimensional integral. We assume that $\psi_K(\mathbf{Q}^{\mathrm{Kramers}},t)$ is identically zero everywhere except along the z axis, and therefore, Eq. (38) may be approximated by

$$\tau_{pzz}^{\mathrm{FENE}} \cong n_p kT - n_p \int Q_z^{\mathrm{Kramers}} F_z^{\mathrm{FENE}}\psi_K(Q_z^{\mathrm{Kramers}},t)\,dQ_z^{\mathrm{Kramers}}, \tag{39}$$

where $\psi_K(Q_z^{\mathrm{Kramers}},t)$ is the distribution function of the z component of the end-to-end *distance*. This is not a good approximation at very low strains when most of the molecules are not yet aligned in the z direction. However, for $\varepsilon > 0.5$ in our uniaxial elongation simulations, the majority of the molecules *do* become aligned with the stretching direction, as evidenced by the fact that values of Q_z are an order of magnitude greater than Q_x or Q_y. Therefore, molecular orientations are limited to a narrow range around the stretching direction, justifying the use of $\psi_K(Q_z^{\mathrm{Kramers}},t)$. The FENE contribution derived above is the stress that would be obtained if there were no strain hardening in the effective end-to-end force, so that the end-to-end force of Kramers chains in strong flows could be described by the FENE force law. The non-FENE contribution is simply defined as the difference between the total stress contribution from the Kramers chains, given by

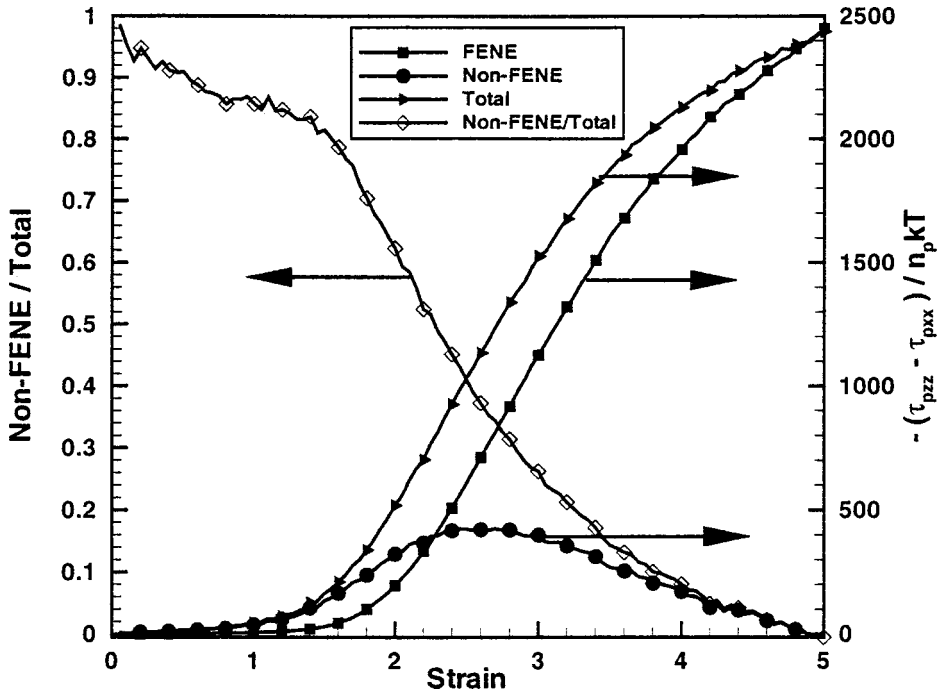

FIG. 8. Partitioning of stress in $N = 41$ Kramers chains into FENE and non-FENE contributions up to $\varepsilon = 5$ in uniaxial extension at Wi = 11.4.

Eq. (12), and the FENE contribution. In Fig. 8, $(\boldsymbol{\tau}_{pzz} - \boldsymbol{\tau}_{pxx})/n_p kT$ is plotted against strain for simulation (2), for which Wi $= 11.38$ and $N = 41$. It should be noted that with the approximation in Eq. (39), $\boldsymbol{\tau}_{pxx}$ is zero at all strains. The evolution of the two components and the ratio of the non-FENE contribution to the total also are shown in Fig. 8.

At $\varepsilon = 5$, the non-FENE component has nearly vanished, and yet the maximum strain hardening is observed at the highest strains in Figs. 6 and 7. This apparent contradiction is easily resolved by recalling that at $\varepsilon = 5$ the distribution function has a large, narrow peak near maximum extension. At that extension, the effective force is almost equal to the FENE force law; and thus, the stress is well approximated by the FENE component. Although there is substantial strain hardening at lower values of Q, there are so few molecules in that part of the configuration space that they contribute very little to the overall stress. In contrast, the non-FENE contribution accounts for 90% of the total stress at $\varepsilon = 0.5$ when the approximation in Eq. (39) becomes valid. The non-FENE contribution in this rapid stretching flow remains high up to strains of approximately 2 when it still accounts for 60% of the total stress. Because the non-FENE contribution to the stress is dominant at low strains, strain hardening in the force law must drive stress growth at these strains. It is possible that a strain-hardening spring force may provide an alternative to a multiple-mode model for capturing the rapid stress growth of a Kramers chain at low strains.

Having established that the effective end-to-end force for a Kramers chain strain hardens, the validity of recent models that modify the force law, stress expression, or both, can be assessed. For example, the force law in the Verhoef model contains an ''elastic'' term, $H(Q^2)\mathbf{Q}$, for which the spring constant is a function of the square of the

end-to-end distance, and a dissipative term, proportional to $(\boldsymbol{\kappa}:\mathbf{QQ})\mathbf{Q}$. The quadratic term is a substitute for the FENE force law, because the authors of this model believe that the nonlinear behavior of the FENE force begins at values of Q that are too large. This leads to the result that the majority of the stress growth occurs at intermediate strains for the FENE dumbbell. The FENE force law also results in an overly sharp knee in the stress–strain curve as it approaches steady state. The use of the quadratic force term removes the sharp knee and gives a smoother approach to steady state. The dissipative term in the force is designed to give more rapid stress growth at low strains. To our knowledge, this is the only kinetic theory model for dilute solutions that contains a force law that depends explicitly on the flow field. However, the Verhoef model predicts a unique value for the force given values for $\mathbf{Q}$ and $\boldsymbol{\kappa}$. In contrast, the simulations in this section reveal that the end-to-end force is not a unique, instantaneous function of $\boldsymbol{\kappa}$ and $\mathbf{Q}$, but that $\mathbf{F}^{(s)}$ depends on the history of these macroscopic and microscopic quantities.

IV. RELAXATION

Doyle *et al.* (1998) noticed that the relaxation of fully stretched Kramers chains and FENE dumbbells, regardless of their maximum length, could be described by a universal curve on a stress–birefringence diagram. We first explain why a universal curve exists for relaxation from full stretch. Next, relaxation dynamics of Kramers chains, FENE dumbbells, and FENE-P dumbbells are explored following extension to a large strain at high Wi. This is not the same as relaxation from full stretch, because relaxation does not start with all the molecules possessing the same (maximum) extension. Instead, it begins from a narrow distribution (e.g., a delta function for the FENE-P dumbbell model) of molecules near Q_0. Nevertheless, the behavior of all three models is demonstrated to be well described by the universal relaxation curve, and an explanation for the agreement of the three models is given. Finally, relaxation is studied following extension up to intermediate strains. At an intermediate strain, there is still a significant number of molecules that are not part of the peak in the distribution function that occurs near maximum extension. The roles of different relaxation mechanisms exhibited by the three models are examined, and an explanation is offered for deviation from the universal relaxation curve.

An ensemble of Kramers chains relaxing from full stretch begins with all of the molecules near maximum extension. In this limit, the end-to-end force is well approximated by the FENE force expression. Since there is no underlying strong flow, the straight chain molecules sample the entire configuration space as they relax. Therefore, the effective force is well approximated by the FENE force law throughout the entire relaxation process, as confirmed in Fig. 9. Figure 9 presents the effective profiles for times 0.2, 0.4, and $0.6\lambda_R$ after the onset of relaxation. In each case, the profile extends over only one or two units of length because at each point in time, the molecules are distributed over a narrow range of lengths. Additionally, the distribution functions for all the models are either Gaussian (for FENE-P) or *nearly* Gaussian (for the Kramers chain and FENE dumbbell) during relaxation from the fully stretched state, as shown in Fig. 10.

Thus the Kramers chain, FENE dumbbell, and FENE-P dumbbell models share two features: the end-to-end distribution functions are Gaussian, and the end-to-end force is well described by the FENE force law. These conditions are *sufficient* for universal relaxation behavior to be exhibited. If the distribution function is always Gaussian, then the polymer stress can be described by the expression for the FENE-P model [Öttinger (1987), (1996)]. Because a Gaussian distribution is fully characterized by its first and second moments, the expression for the FENE force law becomes a function of the configuration tensor, $\langle\mathbf{QQ}\rangle$, as given by

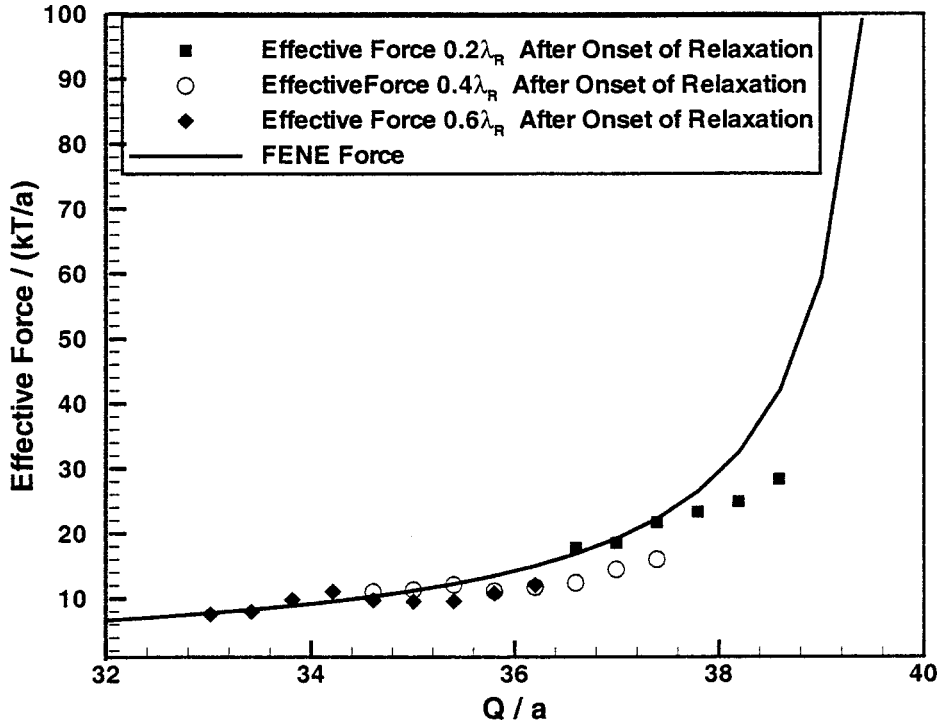

FIG. 9. Evolution of the effective end-to-end force of $N = 41$ Kramers chains and equivalent FENE and FENE-P dumbbells in relaxation from a fully stretched state.

$$\boldsymbol{\tau}_p = n_p kT\boldsymbol{\delta} - n_p H_d \frac{\langle \mathbf{QQ} \rangle}{(1 - \mathrm{tr}(\langle \mathbf{QQ} \rangle)/Q_{0d}^2)}. \tag{40}$$

The birefringence is proportional to the difference in the normal components of $\langle \mathbf{QQ} \rangle$, as expressed by Eq. (20). In a uniaxial extensional flow, the *zz* component of $\langle \mathbf{QQ} \rangle$ is much larger than the *xx* and *yy* components when the extension of the dumbbell is much greater than the equilibrium end-to-end distance. Thus, in this limit, the normal stress difference, the birefringence, and $\mathrm{tr}(\langle \mathbf{QQ} \rangle)$ may all be approximated by the *zz* component of the $\langle \mathbf{QQ} \rangle$ tensor. This leads to the one-to-one, or *universal*, relationship between stress and birefringence given by

$$\Delta\tau_p \cong n_p H_d \frac{\Delta n/K}{(1 - \Delta n/KQ_{0d}^2)}, \tag{41}$$

where $K = 5Cn_p kT(N-1)/Q_{0d}^2$ is the prefactor to the summation in Eq. (20).

A comparison of the stress–birefringence relaxation behavior of the Kramers chain, FENE dumbbell, and the FENE-P dumbbell models following an extension to $\varepsilon = 5$ at $\mathrm{Wi} = 11.4$ [simulation (2)] is shown in Fig. 11. The relaxation (and extension) behavior of the FENE-P chain is given by the universal relaxation curve, because its distribution function is always Gaussian and its end-to-end force law is always given by the FENE spring expression. The relaxation behaviors of the FENE dumbbell and Kramers chain also are well described by the universal relaxation curve. The evolution of the distribution functions for the three models is compared in Fig. 12 to understand why the FENE dumbbell and the Kramers chain follow the universal relaxation curve. At the instant the

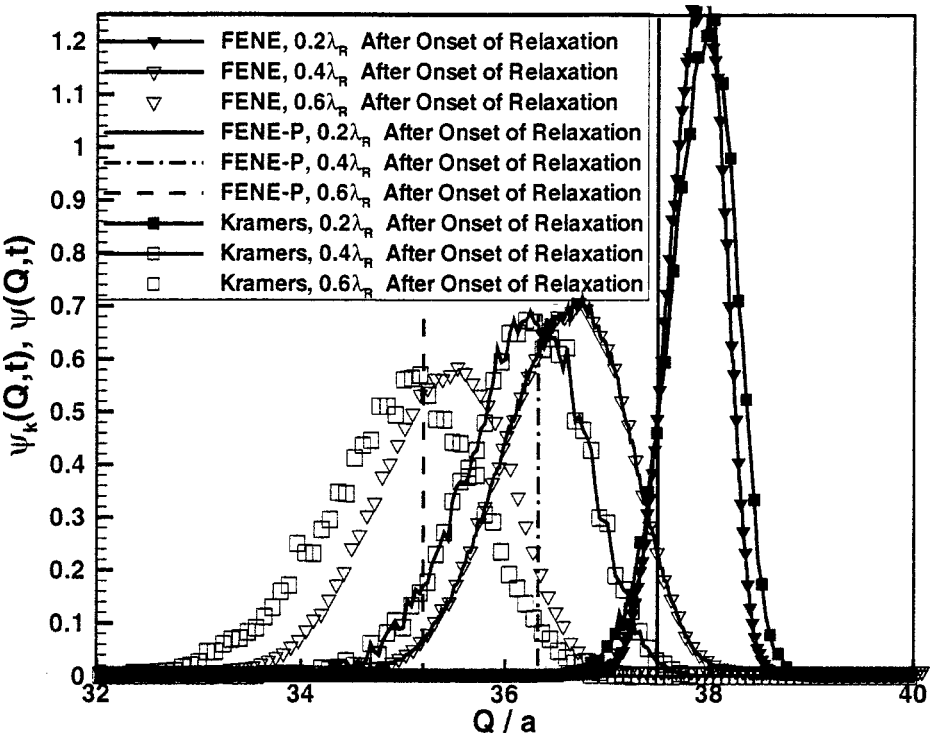

FIG. 10. Evolution of the end-to-end distribution function of $N = 41$ Kramers chains and equivalent FENE and FENE-P dumbbells in relaxation from a fully stretched state.

flow is turned off, all three models have very narrow, peaked distributions near maximum extension. The distribution function for the FENE-P model is represented as a delta function in this plot. However, as noted by Öttinger (1996), the FENE-P dumbbell model also can be derived by assuming a Gaussian distribution. Thus, the distribution function of the FENE-P dumbbell in Fig. 12 can be interpreted as being a Gaussian function with a maximum value that corresponds to the delta functions shown in Fig. 12. During relaxation, the peaks for all three models migrate to equilibrium. As the relaxation progresses, the distribution functions for the FENE dumbbell and Kramers chain become shorter and broader, but always assume a symmetric Gaussian shape. The distribution function of the FENE dumbbell remains higher and narrower than that of the Kramers chain, because the peak of the FENE distribution function is higher at the end of the extension phase, and the difference persists during relaxation. Because an ensemble of FENE dumbbells is identical to an ensemble of FENE-P dumbbells when the end-to-end distribution function is Gaussian, we expect the FENE dumbbell model to relax according to the universal relaxation curve.

The end-to-end distribution function of the Kramers chain also appears Gaussian during relaxation, but for this model to relax according to the universal relaxation curve, the effective end-to-end force must be near the FENE result for the majority of the chains. After extension at Wi = 11.4 up to $\varepsilon = 5$, the narrow peak of the end-to-end distribution function of the Kramers chains extends from $38.8a \leqslant Q \leqslant 39.5a$ as shown in Fig. 13(a). This peak contains over 95% of the molecules, and over this range the effective force in the Kramers chain is very close to the FENE value. As the relaxation progresses, the effective force at a given Q must relax to its FENE value before the peak

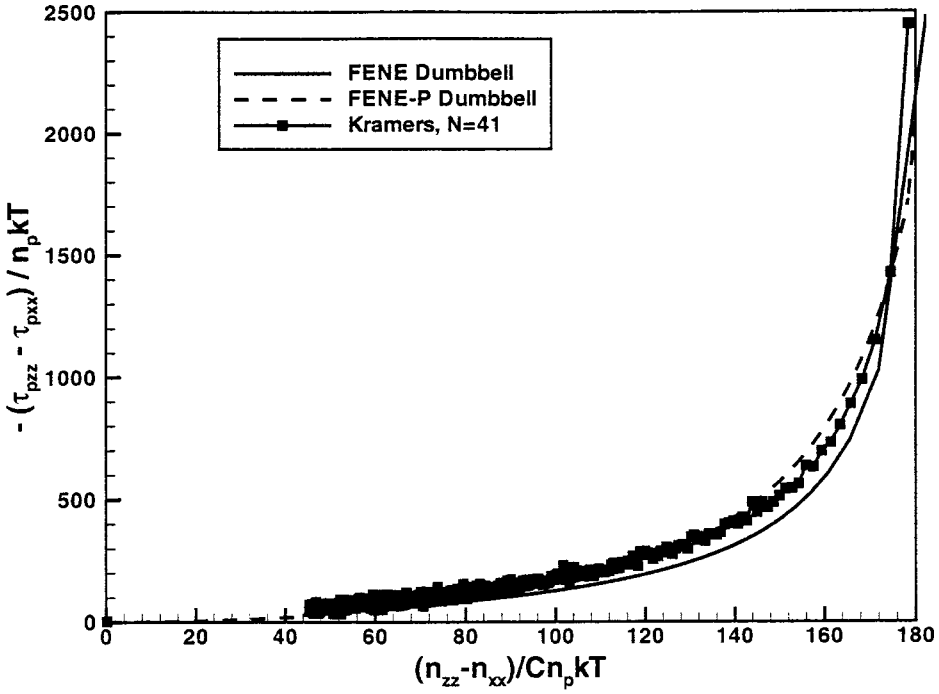

FIG. 11. Dependence of stress on birefringence for $N = 41$ Kramers chains and equivalent FENE and FENE-P dumbbells in relaxation following uniaxial extension to $\varepsilon = 5$ at Wi $= 11.4$.

of $\psi_K(Q,t)$ reaches that Q. If this occurs, then the majority of the Kramers chains will experience an effective force that is FENE-like, and the Kramers chain will relax according to the universal relaxation curve. The relaxations of the distribution function and effective force profile for the Kramers chain up to $0.3\lambda_R$ after the cessation of flow are shown in Figs. 13(a) and 13(b), respectively. Notice that the effective force has relaxed approximately to the level of the FENE level for values of Q at which the peak of $\psi_K(Q,t)$ is located. The effective force profile dips below the FENE force profile at the largest values of Q. This is not surprising because the FENE force law is an approximation to the inverse Langevin function. As expected, the effective force profiles tend to the inverse Langevin limit for large extensions.

It should be emphasized that the relaxation of the effective force profiles is extremely fast relative to the rate for strain hardening [Orr and Sridhar (1996)]. The rapidity of the relaxation is crucial in order for the Kramers chain behavior to be described by the universal relaxation curve. Snapshots of the effective force profiles during relaxation following an extension to $\varepsilon = 5$ at Wi $= 11.4$ are shown in Fig. 14. The effective force profile at the instant the flow is turned off is shown by the uppermost curve; it takes a time of $10\lambda_R$ to strain harden the force profile to this extent. However, in the relaxation portion of the experiment, the strain-hardened force profile has relaxed very close to the FENE force law within a time of $2\lambda_R$ from the cessation of the stretching phase of the experiment. Thus, the chains that are not fully stretched out, e.g., the kinked configurations that build up during stretching and lead to large effective forces, relax very quickly.

In relaxation following stretching to an intermediate strain, the relaxation of the effective forces plays a far more important role. The evolution of the distribution functions of 40-rod Kramers chains and equivalent FENE dumbbells following an extension to

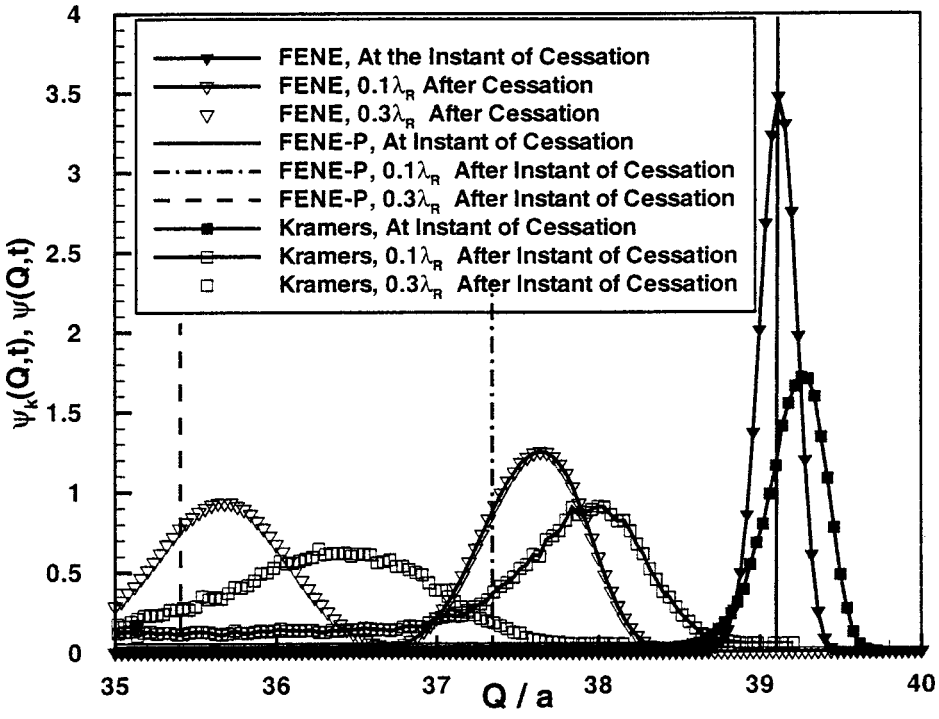

FIG. 12. Relaxation of the end-to-end distribution of $N = 41$ Kramers chains and equivalent FENE and FENE-P dumbbells in relaxation following uniaxial extension to $\varepsilon = 5$ at Wi = 11.4.

$\varepsilon = 2.5$ at Wi = 11.4 is shown in Fig. 15. For FENE dumbbells, about 80% of the ensemble are part of the peak at large extensions. Because 20% of the dumbbells have not undergone the coil–stretch transition, the overall distribution is not Gaussian. Thus, the relaxation behavior of the FENE dumbbell is expected to deviate from the universal curve; this is confirmed in Fig. 16. For Kramers chains, 60%–70% of the molecules have $Q < 30a$ at the beginning of relaxation. The shape of the distribution function for $Q < 30a$ also does not change significantly for times less than $0.5\lambda_R$ following the onset of relaxation; however, as shown in Fig. 17, the effective forces for $Q < 30a$ decay dramatically in that time period. Thus, the relaxation of the Kramers chain from $\varepsilon = 2.5$ is different than the relaxation from $\varepsilon = 5$ for two reasons. First, at the beginning of the relaxation, there are many molecules that have not undergone the coil–stretch transition. Second, the effective end-to-end forces in the molecules that have not unraveled completely deviate markedly from the FENE force law and also decrease during the relaxation. The result is that the stress–birefringence behavior of the FENE dumbbell and of the Kramers chain both deviate significantly from the universal curve.

V. STRESS–BIREFRINGENCE HYSTERESIS

Lielens *et al.* (1999) have discussed sources of hysteresis for an ensemble of FENE dumbbells. Here, we examine the hysteresis of FENE chains and Kramers chains. The hysteresis of a Kramers chain is composed of two components that we refer to as *distributional hysteresis* and *configurational hysteresis*. The distributional component of hysteresis arises because $\psi_K(Q,t)$ has a non-Gaussian shape during extension (Fig. 4). As was shown in Sec. IV, a non-Gaussian distribution leads to a deviation from the universal

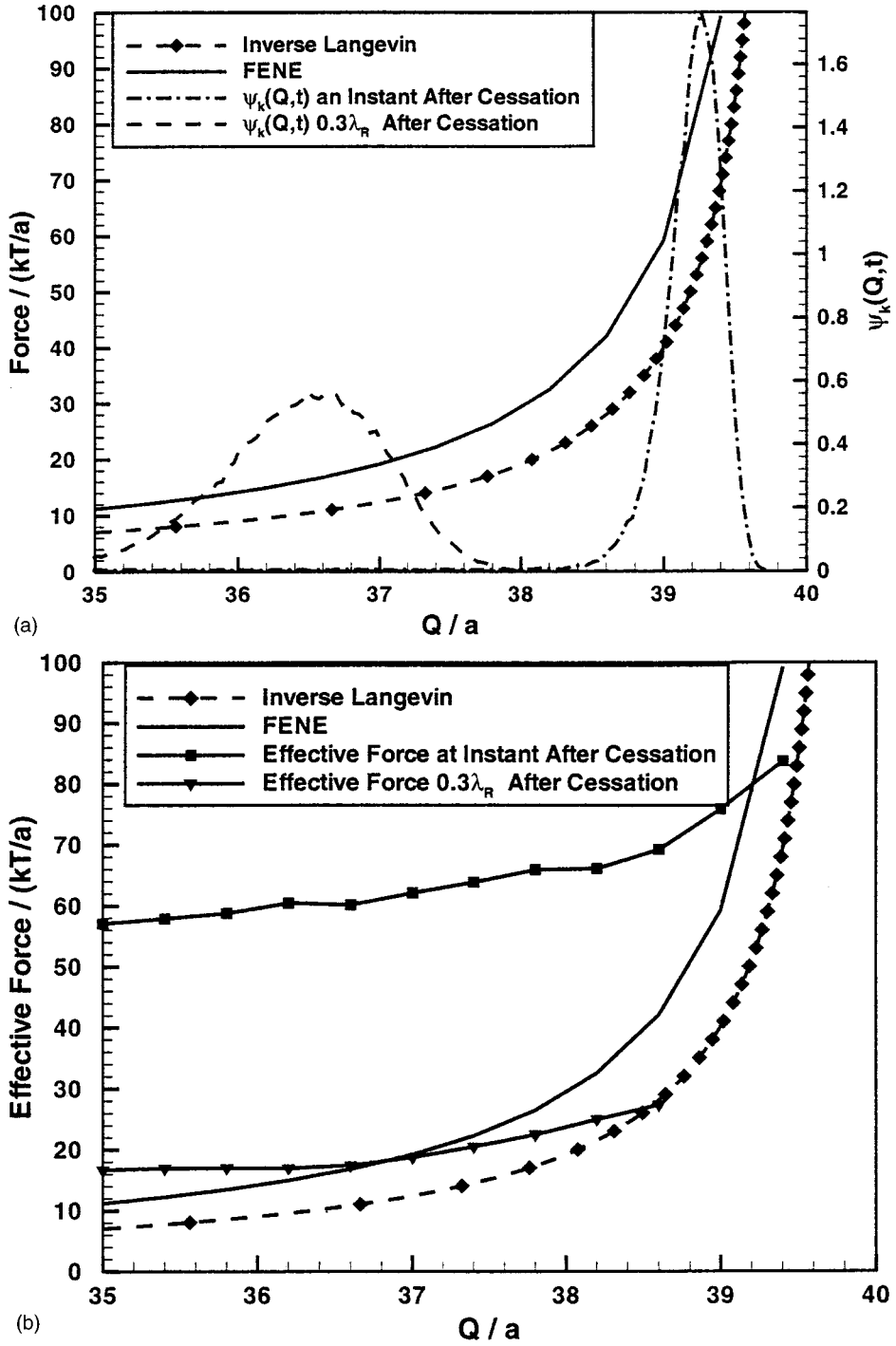

FIG. 13. (a) Relaxation of the end-to-end distribution functions for $N = 41$ Kramers chains and equivalent FENE and FENE-P dumbbells in relaxation following uniaxial extension to $\varepsilon = 5$ at Wi = 11.4. (b) Relaxation of the effective end-to-end force profiles for $N = 41$ Kramers chains and equivalent FENE and FENE-P dumbbells in relaxation following uniaxial extension to $\varepsilon = 5$ at Wi = 11.4.

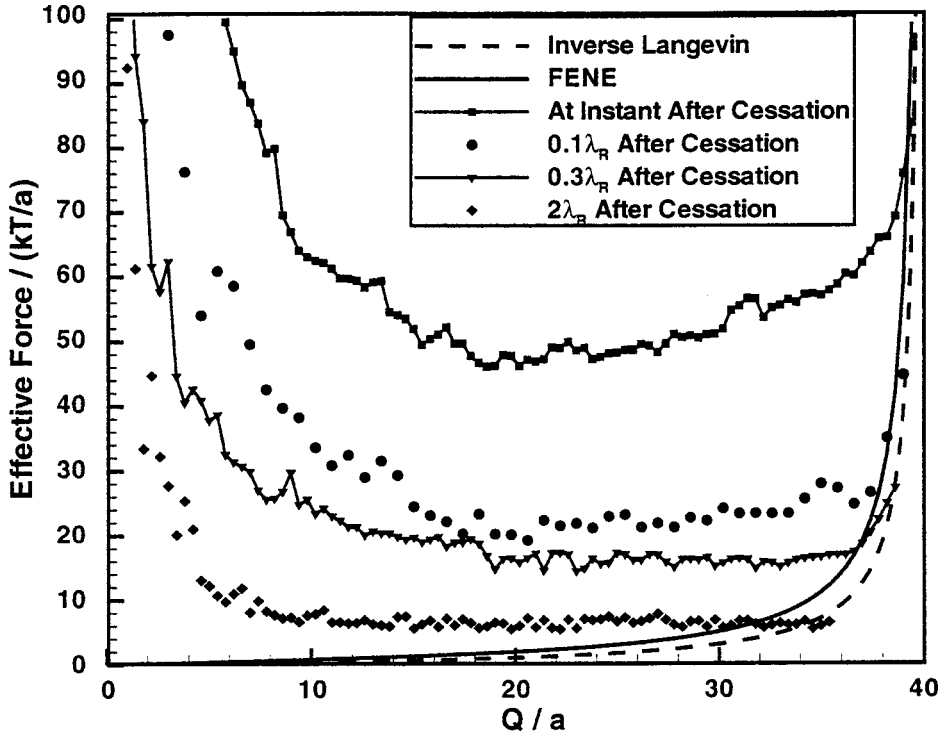

FIG. 14. Relaxation of the end-to-end effective force in $N = 41$ Kramers chains in relaxation following uniaxial extension to $\varepsilon = 5$ at Wi = 11.4.

relaxation curve. If the extensional arm of the stress–birefringence diagram is different from the universal relaxation curve, the model will predict hysteresis. The hysteresis of the FENE dumbbell is due to this *distributional* component alone. However, the Kramers chain has an added *configurational* component to hysteresis. The notion of configurational hysteresis was first described by Doyle *et al.* (1998) to be associated with the fact that molecules assume different configurations during extension and relaxation. However, no method has been provided to separate the two types of hysteresis or to estimate their relative magnitudes. We describe below a methodology that can achieve both of these objectives. The effective end-to-end force in Kramers chains was shown in Fig. 14 to evolve at different rates during extension and relaxation. The calculation of the effective end-to-end forces involves dividing the total stress in a bin by the number of molecules in that bin. Thus, the effective force contains no information about the distribution function, and any difference in the evolution of the effective force during extension and relaxation will contribute additional hysteresis to the system independent of distributional effects. This additional component of hysteresis is identified as configurational in origin because the deviation of the effective force from the FENE force law is driven by the formation of kinked internal configurations that arise from the underlying strong flow.

The relative magnitudes of configurational and distributional hysteresis are estimated by comparing the stress–birefringence plot for Kramers chains with that which *would be* generated if the end-to-end force in the Kramers chains were always of FENE character. These plots are shown in Fig. 18 for a system that was elongated at Wi = 11.4 up to

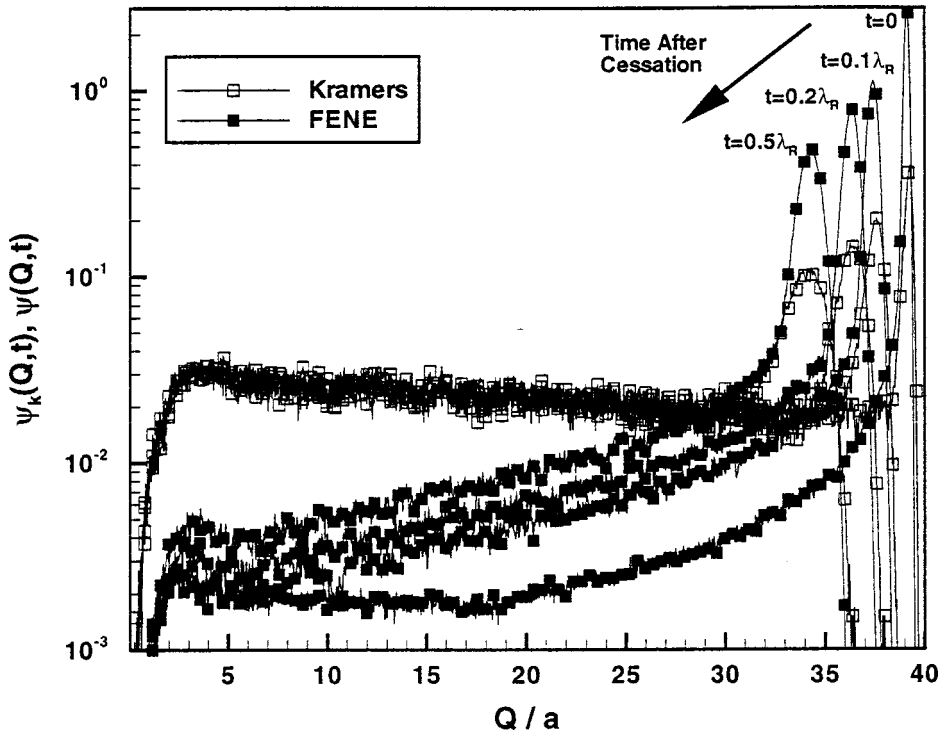

FIG. 15. Relaxation of the end-to-end distribution functions of $N = 41$ Kramers chains and equivalent FENE dumbbells in relaxation following uniaxial extension to $\varepsilon = 2.5$ at Wi = 11.4.

$\varepsilon = 5$. The difference between the enclosed areas of the two plots for Kramers chains is the configurational contribution to hysteresis and is a major contributor to the overall hysteresis.

The shapes of the stress–birefringence hysteresis loops for FENE dumbbells and Kramers chains are very similar, but the hysteresis is slightly greater for the FENE dumbbell model. This contrasts with hysteresis in stress and the root-mean-square end-to-end distance $\langle Q^2 \rangle^{1/2}$. Figure 19 shows that the extension arm of the stress versus $\langle Q^2 \rangle^{1/2}$ plot rises more steeply for the Kramers chain model at small values of $\langle Q^2 \rangle^{1/2}$; and the Kramers chain shows more hysteresis than the FENE dumbbell. This is because the root-mean-square end-to-end distance $\langle Q^2 \rangle^{1/2}$, which is closely related to birefringence for the FENE dumbbell, grows faster for FENE dumbbells than for Kramers chains (Fig. 3), but stress grows more slowly (see Fig. 1). To understand why the FENE dumbbell model exhibits more hysteresis in stress versus birefringence but less hysteresis in stress versus $\langle Q^2 \rangle^{1/2}$, the hysteresis of the two models in birefringence versus $\langle Q^2 \rangle^{1/2}$ is considered in Fig. 20. The Kramers chain exhibits hysteresis in the birefringence versus $\langle Q^2 \rangle^{1/2}$ diagram, whereas the FENE dumbbell cannot because birefringence is a unique function of $\langle Q^2 \rangle^{1/2}$.

The FENE dumbbell does not exhibit hysteresis in the behavior of birefringence with $\langle Q^2 \rangle^{1/2}$ because both birefringence and $\langle Q^2 \rangle^{1/2}$ are closely approximated by the *zz* component of $\langle \mathbf{QQ} \rangle$ for large extensions. Hence, there is a one-to-one mapping between $\langle Q^2 \rangle^{1/2}$ and birefringence. The birefringence of the Kramers chain, on the other hand, displays extremely rapid initial growth with $\langle Q^2 \rangle^{1/2}$. This is because birefringence measures the degree of alignment of the chain segments with the stretching direction. *For*

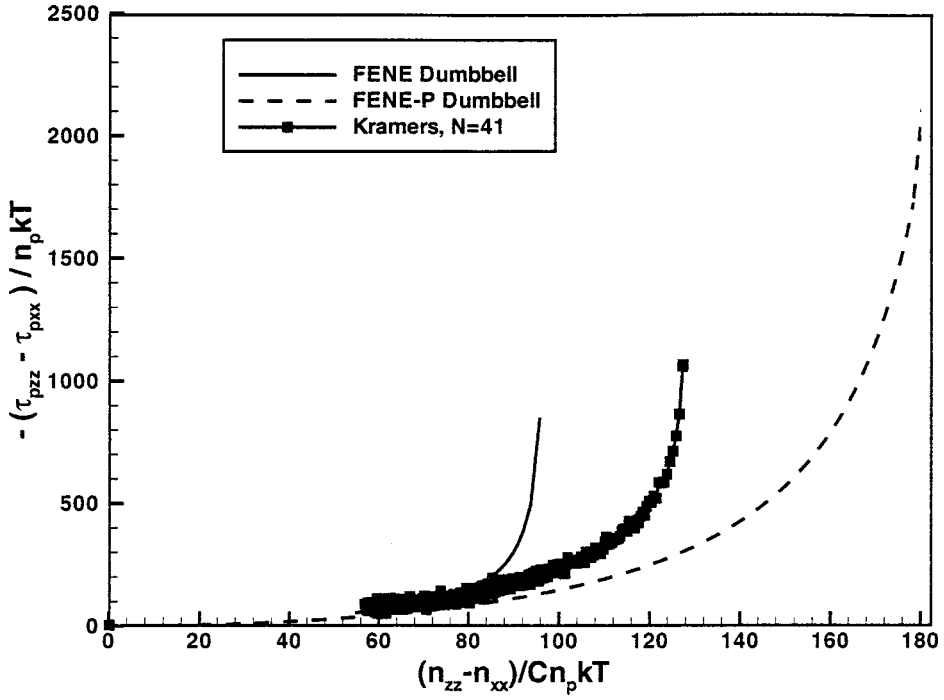

FIG. 16. Dependence of stress on birefringence for $N = 41$ Kramers chains and equivalent FENE dumbbells during relaxation following uniaxial extension to $\varepsilon = 2.5$ at Wi = 11.4.

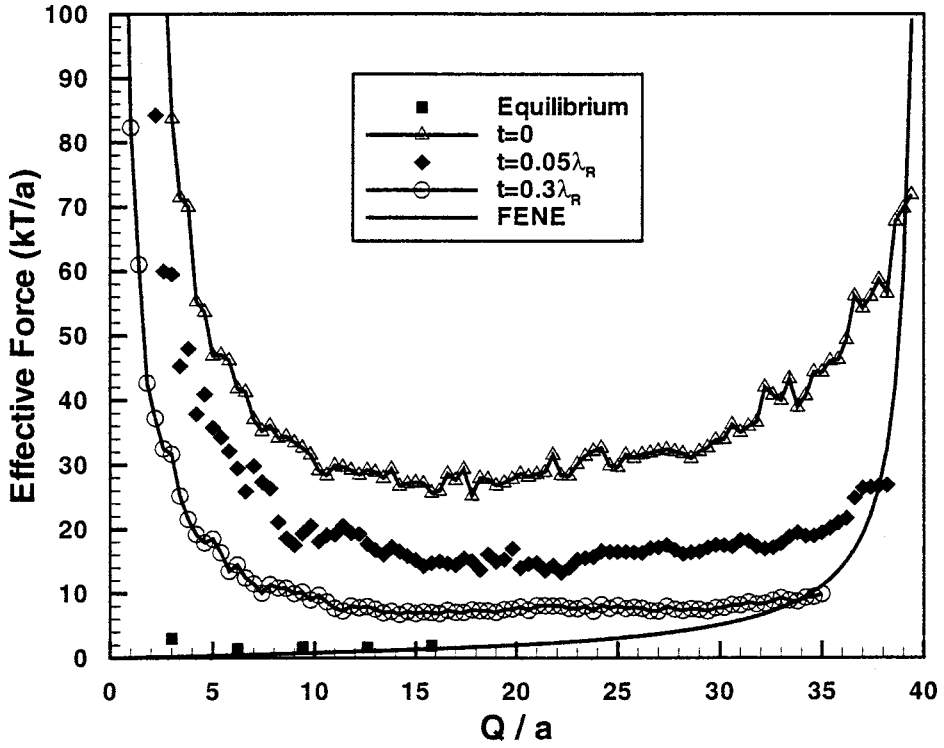

FIG. 17. Relaxation of the end-to-end effective force in $N = 41$ Kramers chains in relaxation following uniaxial extension to $\varepsilon = 2.5$ at Wi = 11.4.

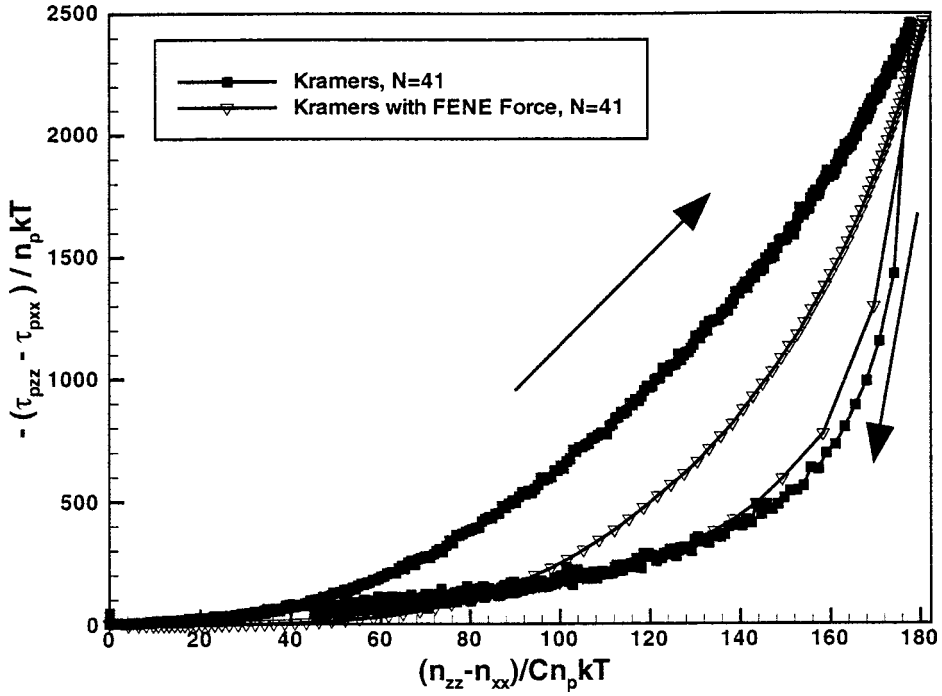

FIG. 18. Dependence of stress on birefringence in uniaxial extension to $\varepsilon = 5$ at Wi = 11.4 and in subsequent relaxation for $N = 41$ Kramers chains and $N = 41$ Kramers chains whose end-to-end forces are set equal to the FENE force law.

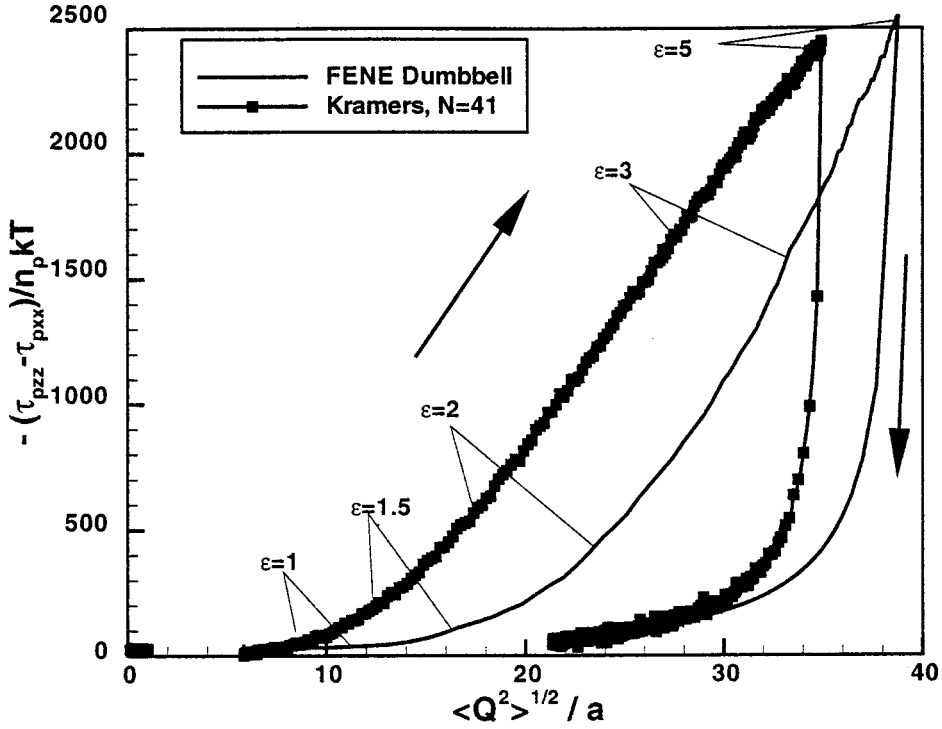

FIG. 19. Dependence of stress on $\langle Q^2 \rangle^{1/2}$ for $N = 41$ Kramers chains and equivalent FENE dumbbells in uniaxial extension to $\varepsilon = 5$ at Wi = 11.4 and in subsequent relaxation.

Kramers chains, alignment at the segmental level begins immediately and can occur independently of any growth in $\langle Q^2 \rangle^{1/2}$.

Another important difference between the hysteresis behavior of FENE dumbbells and Kramers chains is the rate at which the stress–birefringence hysteresis loops are traversed. The stress–birefringence curve shown in Fig. 21 is traversed more quickly for the Kramers chain. Thus, if the extension is terminated at an intermediate strain, the Kramers chain will exhibit more hysteresis because it has climbed to a higher point on the extension arm of the curve. For the short chains examined in this study, there is a significant difference between the rates at which the hysteresis loops are traversed up to $\varepsilon \simeq 2.5$.

The rate at which the hysteresis loops are traversed is very important for comparison with experimental data. Doyle *et al.* showed that a FENE dumbbell greatly underpredicts the experimentally observed hysteresis in an experiment conducted to a strain of about 4. The results in this paper suggest that if a 2850-rod Kramers chain could be simulated, it would predict much more hysteresis than the FENE dumbbell and might agree more closely with experiments.

VI. FENE CHAINS

In strong extensional flows, the deviation of the effective end-to-end force for a Kramers chain from the FENE force law was attributed to the entire chain's inability to sample its full configuration space before being deformed by the underlying flow. However, if a Kramers chain consisting of N rods were approximated by a FENE chain consisting of M springs, each spring would now represent a far smaller segment of the Kramers chain, N/M rods. Since these segments have a smaller configuration space to sample, we expect that the FENE force law is a better approximation for these segments than for the full Kramers chain. Hence, the FENE chain should be a better approximation than a FENE dumbbell to the Kramers chain in terms of describing transient stress growth and hysteresis. The validity of this claim is examined in this section.

Plots of stress and birefringence as functions of strain for FENE chains are shown in Figs. 22 and 23, respectively, for calculations with 2, 3, and 6 springs. The uniaxial extension is conducted at $\mathrm{Wi} = 11.4$, and the product $M \times b_s$ is kept constant at 120. Hence, these FENE chains represent a 40-rod Kramers chain, according to Eq. (30). The behavior of the Kramers chain and FENE dumbbell also are included on Figs. 22 and 23 for comparison. As more modes are added, there is faster growth in stress and birefringence at low strains. In fact, the 6-spring FENE chain agrees well with the predictions of the Kramers chain over the entire range of strains. All the models predict the same steady-state values of stress and birefringence.

The dynamics of the stress and birefringence of a 6-spring FENE chain, a Kramers chain, and a FENE dumbbell are compared in Fig. 24 for uniaxial elongation up to $\varepsilon = 5$ at $\mathrm{Wi} = 11.4$, followed by relaxation. The hysteresis curve of the 6-spring FENE chain coincides with that for the Kramers chain. The FENE chain also traverses its hysteresis loop at a similar rate to the Kramers chain, but much faster than the FENE dumbbell.

Plots of birefringence as a function of $\langle Q^2 \rangle^{1/2}$ are shown in Fig. 25 for the 6-mode FENE chain, Kramers chain, and FENE dumbbell. As for the Kramers chain, the multiple modes of the FENE chain enable it to exhibit hysteresis in birefringence versus $\langle Q^2 \rangle^{1/2}$. Overall, the FENE chain predicts transient rheology and hysteresis that agree more closely with the Kramers chain than do the predictions of the FENE dumbbell.

VII. CONCLUSIONS

This work highlights the inability of the inverse Langevin function (or the FENE approximation to it) to describe the effective end-to-end force in a Kramers chain in strong, transient uniaxial elongational flows. As strain increases in such flows, the *entire* effective end-to-end force *profile* of the Kramers chain assumes larger values than those given by the FENE force law. We refer to this effect as strain hardening. Moreover, we find that the rate of strain hardening increases with the strain rate. The percentage of deviation of the effective force from the FENE force decreases with increasing end-to-end length and tends to zero at maximum extension. When the extensional flow is turned off, the rate at which the effective force relaxes back to the FENE force law is much greater than the rate at which it strain hardens. Consequently, it has been demonstrated that the effective end-to-end force *profile* depends strongly on the deformation history. This behavior is far more complex than is reflected in any single-mode molecular model currently in use.

The effective end-to-end force of the Kramers chain deviates from the inverse Langevin function, because the latter function assumes that the polymer chain is always locally equilibrated. However, this is not the case for Kramers chains in a rapid stretching flow for which a large fraction of molecules possess conformations such that the end-to-end force is not described by the inverse Langevin function. These nonlocally equilibrated conformations disappear very rapidly during relaxation, and consequently, the effective end-to-end force returns to the FENE force law very soon after the cessation of an extensional flow.

The strain-history dependence of the effective force profile measured for a Kramers chain also helps to clarify several effects associated with extensional flows. First, the nature of this strain-history-dependent effective force profile allows us to characterize fully the previously qualitative notion of configurational hysteresis. The FENE dumbbell model, which has a force law that is a function of molecular end-to-end distance only, can exhibit distributional hysteresis but not configurational hysteresis. However, if a dumbbell model possesses a strain-history-dependent end-to-end force profile, as observed for the Kramers chain, configurational hysteresis can be generated because the force profile evolves differently during extension and relaxation. Second, we show that the evolution of the effective force profile following the cessation of extension is not consistent with the stress jumps that are a feature of the Hinch, Rallison, and Verhoef models. Though rapid, the relaxation of the effective force profile of the Kramers chain following the cessation of elongational flow is not instantaneous. Therefore, a dumbbell model that possesses this type of strain-history-dependent force law does not exhibit stress jumps. Third, we show that a strain-hardening effective force profile accounts for the rapid stress growth in start up of steady elongational flow that is observed for the Kramers chain but not for the FENE dumbbell. A dumbbell model with an end-to-end force profile that strain hardens in the same way as that observed for the effective force of the Kramers chain will predict a more rapid rate of stress growth in the start up of elongation than a model with a constant force law, such as the FENE dumbbell.

The end-to-end distribution functions of the Kramers chain and FENE dumbbell evolve through a qualitatively similar set of shapes during extension and relaxation. The peak of the FENE dumbbell distribution function migrates to full extension faster than that of the Kramers chain, suggesting that the FENE spring force is too small. However, if the FENE force were replaced by a strain-hardening force as observed for the Kramers chain, it is likely that the larger force would slow the migration of the peak of the end-to-end distribution function to larger extensions for the FENE dumbbell. Hence, the

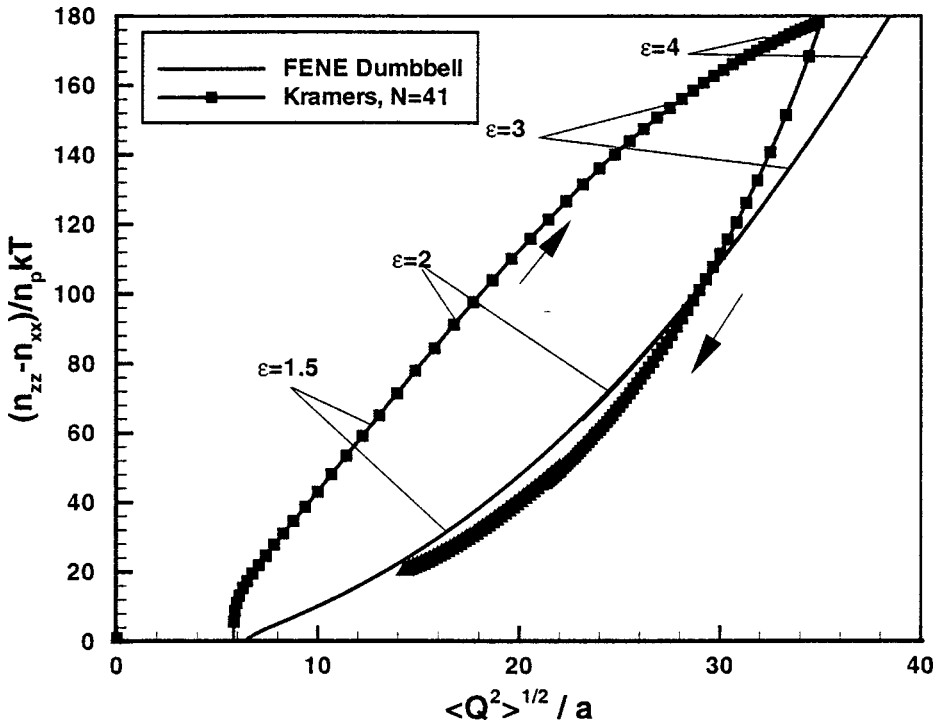

FIG. 20. Dependence of birefringence on $\langle Q^2\rangle^{1/2}$ for $N = 41$ Kramers chains and equivalent FENE dumbbells in uniaxial extension to $\varepsilon = 5$ at Wi = 11.4 and in subsequent relaxation.

evolution of the end-to-end distribution function would be more closely matched for the two models. Consequently, it appears that using the same force law in the Fokker–Planck equation and in the stress tensor expression is not only consistent with the kinetic theory framework, but may also yield a better match between the Kramers chain and a dumbbell model in the description of the evolution of the end-to-end distribution function. This contrasts with the model used by Rallison (1996) that employs different force expressions in the Fokker–Planck and stress equations.

This paper also demonstrates that FENE chains better predict the transient stress growth *and* hysteresis of Kramers chains than do FENE dumbbells. This is in contrast to the FENE-PM approximation to the FENE chain, which does not predict hysteresis. Li and co-workers (2000) have further validated the FENE chain as a good model for dilute polymer solutions by demonstrating that it agrees well with experimental observations of transient stress growth and hysteresis.

To place this work in the context of complex flow simulations of polymer solutions, this paper has shown two ways to coarse grain the Kramers chain. First, we show that if the model is restricted to a single configurational variable, such as the end-to-end vector, then the spring force *profile* must vary with deformation history. If such a model were used in a complex flow simulation, computational effort could be saved since short time-scale behavior could be captured with a model with only one configurational variable. However, although we characterize the behavior of the deformation-history-dependent force profile in the start up of and the relaxation following elongational flow, we are unable to describe the evolution of the effective force profiles in a simple mathematical formulation. We suspect that any mathematical description of the behavior of

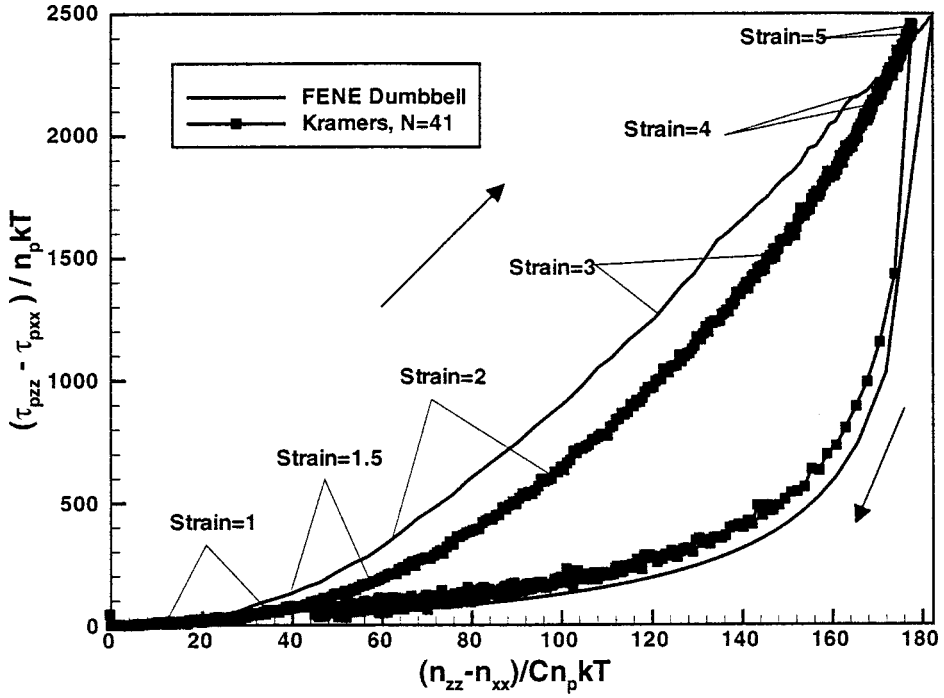

FIG. 21. Dependence of stress on birefringence for $N = 41$ Kramers chains and equivalent FENE dumbbells in uniaxial extension to $\varepsilon = 5$ at Wi = 11.4 and in subsequent relaxation. The points along the extension segment reached at various strains are marked for both models.

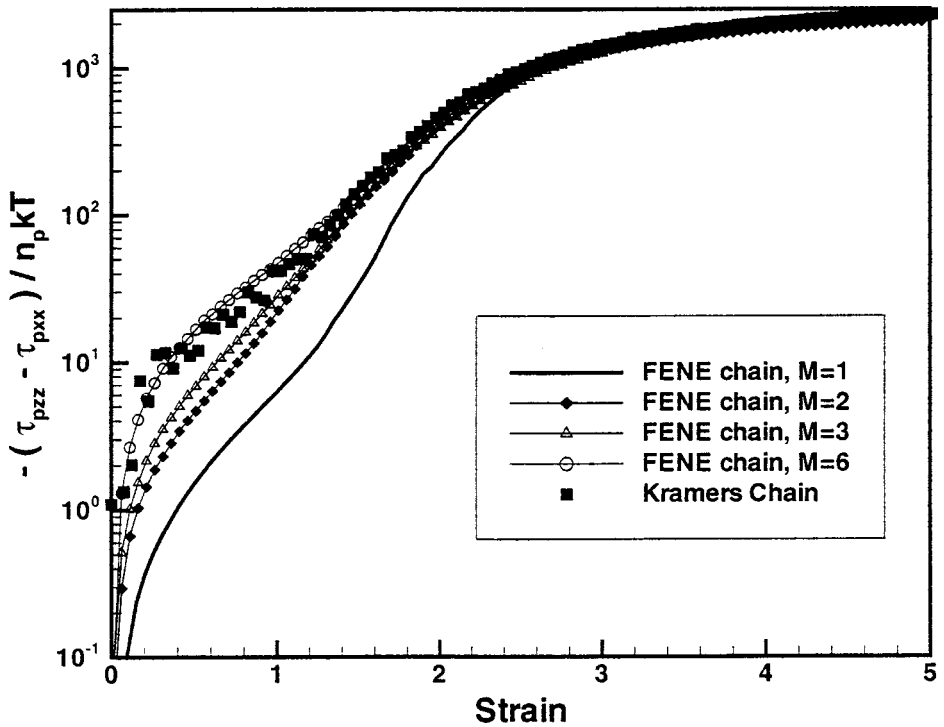

FIG. 22. Dependence of stress on strain for $N = 41$ Kramers chains and equivalent 1-, 2-, 3-, and 6-spring FENE chains in uniaxial extension at Wi = 11.4.

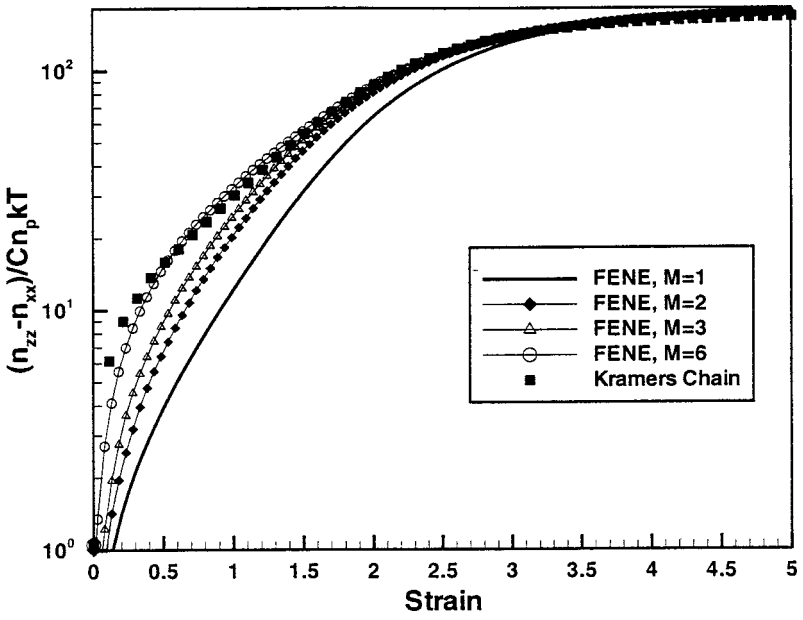

FIG. 23. Dependence of birefringence on strain for $N = 41$ Kramers chains and equivalent 1-, 2-, 3-, and 6-spring FENE chains in uniaxial extension at Wi = 11.4.

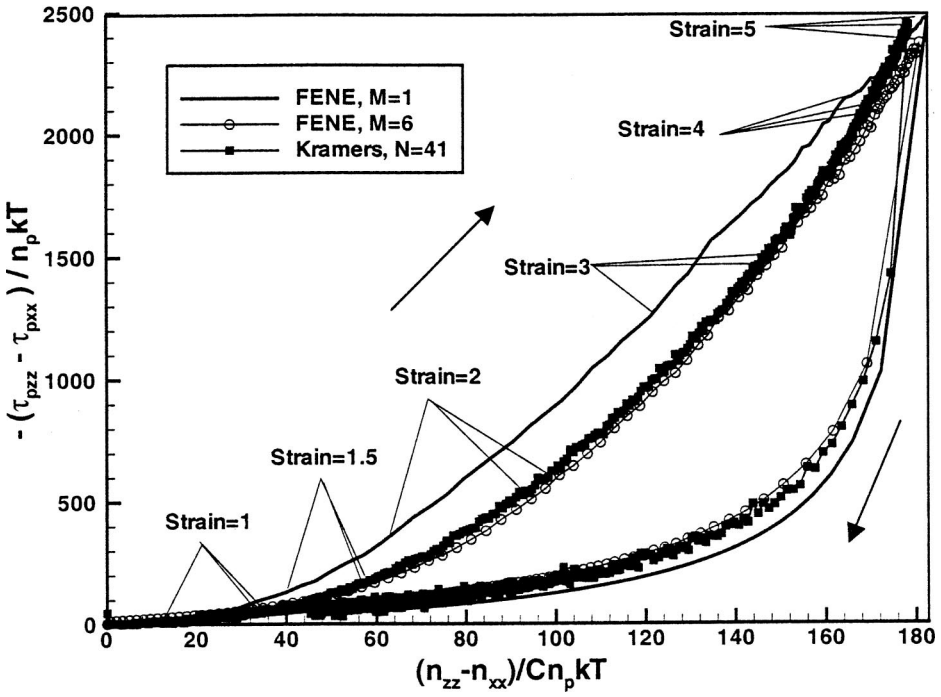

FIG. 24. Dependence of stress on birefringence for $N = 41$ Kramers chains, equivalent FENE dumbbells, and 6-spring FENE chains in uniaxial extension up to $\varepsilon = 5$ at Wi = 11.4 and in subsequent relaxation.

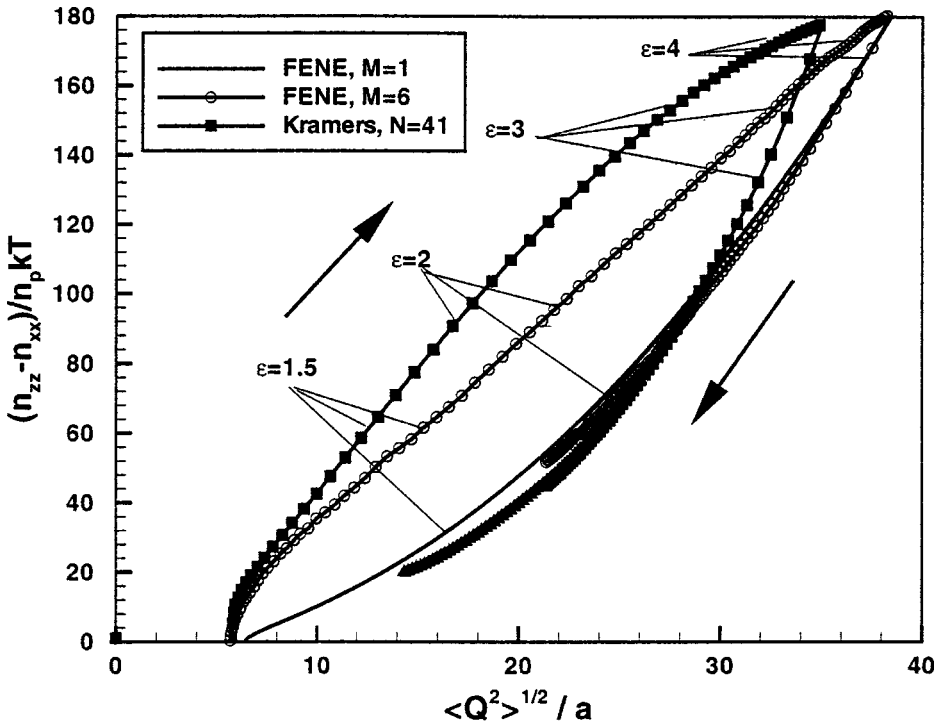

FIG. 25. Dependence of birefringence on $\langle Q^2\rangle^{1/2}$ for $N = 41$ Kramers chains, equivalent FENE dumbbells, and 6-spring FENE chains in uniaxial extension up to $\varepsilon = 5$ at Wi = 11.38 and in subsequent relaxation.

the force profiles for general flows will be too complicated to be numerically tractable in a complex flow calculation. The second method for coarse graining is to use a multimode bead-spring model in which the spring force is given by the FENE force law. However, although the FENE chain is conceptually simple, the simulation of multiple-mode models is currently too computationally expensive in complex flow calculations. Therefore, there is a great need for a dumbbell model that captures fine length scale physics without requiring a complicated deformation-dependent force law.

ACKNOWLEDGMENT

This work was supported primarily by the ERC Program of the National Science Foundation under Award No. EEC-9731680.

References

Bird, R. B., C. F. Curtiss, R. C. Armstrong, and O. Hassager, *Dynamics of Polymeric Liquids, Kinetic Theory*, 2nd ed. (Wiley Interscience, New York, 1987), Vol. 2.

Doyle, P. S., E. S. G. Shaqfeh, and A. P. Gast, ''Dynamic simulation of freely draining flexible polymers in steady linear flows,'' J. Fluid Mech. **334**, 251–291 (1997).

Doyle, P. S. and E. S. G. Shaqfeh, ''Dynamic simulation of freely draining, flexible bead-rod chains: Startup of extensional and shear flow,'' J. Non-Newtonian Fluid Mech. **76**, 43–78 (1998).

Doyle, P. S., E. S. G. Shaqfeh, G. H. McKinley, and S. H. Spiegelberg, ''Relaxation of dilute polymer solutions following extensional flows,'' J. Non-Newtonian Fluid Mech. **76**, 79–110 (1998).

Flory, P. J., *Principles of Polymer Chemistry* (Cornell University, Ithaca, NY, 1953).

Gardiner, C. W., *Handbook of Stochastic Methods* (Springer, Berlin, 1985).
Ghosh, I., Ph.D. Thesis, Massachusetts Institute of Technology, Cambridge (2000).
Herrchen, M. and H. C. Öttinger, ''A detailed comparison of various FENE dumbbell models,'' J. Non-Newtonian Fluid Mech. **68**, 17–42 (1997).
Hinch, E. J., ''Uncoiling a polymer molecule in a strong extensional flow,'' J. Non-Newtonian Fluid Mech. **54**, 209–230 (1994).
James, D. F. and T. Sridhar, ''Molecular conformation during steady-state measurements of extensional viscosity,'' J. Rheol. **39**, 713–724 (1995).
Keunings, R., ''On the Peterlin Approximation for finitely extensible dumbbells,'' J. Non-Newtonian Fluid Mech. **68**, 85–100 (1997).
Larson, R. G., H. Hu, D. E. Smith, and S. Chu, ''Brownian dynamics simulations of a DNA molecule in an extensional flow field,'' J. Rheol. **43**, 267–304 (1999).
Lielens, G., R. Keunings, and V. Legat, ''The FENE-L and the FENE-LS closure approximations to the kinetic theory of finitely extensible dumbbells,'' J. Non-Newtonian Fluid Mech. **87**, 179–196 (1999).
Li, L., R. G. Larson, and T. Sridhar, ''Brownian dynamics simulations of dilute polystyrene solutions,'' J. Rheol. **44**, 291–322 (2000).
Li, L. and R. G. Larson, ''Excluded volume effects on the birefringence and stress of dilute polymer solutions in extensional flow,'' Rheol. Acta **39**, 419–427 (2000).
Liu, T. W., ''Flexible polymer chain dynamics and rheological properties in steady flows,'' J. Chem. Phys. **90**, 5826–5842 (1989).
Orr, N. V. and T. Sridhar, ''Stress relaxation in uniaxial extension,'' J. Non-Newtonian Fluid Mech. **67**, 77–103 (1996).
Öttinger, H. C., ''A model of dilute polymer solutions with hydrodynamic interaction and finite extensibility. I. Basic equations and series expansions,'' J. Non-Newtonian Fluid Mech. **26**, 207–246 (1987).
Öttinger, H. C., *Stochastic Processes in Polymeric Fluids* (Springer, Berlin, 1996).
Perkins, T. T., D. E. Smith, and S. Chu, ''Single polymer dynamics in an extensional flow,'' Science **276**, 2016–2021 (1997).
Rallison, J. M., ''Dissipative stresses in dilute polymer solutions,'' J. Non-Newtonian Fluid Mech. **68**, 61–83 (1996).
Rallison, J. M. and E. J. Hinch, ''Do we understand the physics in the constitutive equation?,'' J. Non-Newtonian Fluid Mech. **29**, 37–55 (1988).
Schieber, J. D. and H. C. Öttinger, ''On the consistency criteria for stress tensors in kinetic theory models,'' J. Rheol. **38**, 1909–1924 (1994).
Sizaire, R., G. Lielens, I. Jaumain, R. Keunings, and V. Legat, ''On the hysteretic behavior of dilute polymer solutions in relaxation following extensional flow,'' J. Non-Newtonian Fluid Mech. **82**, 233–253 (1999).
Smith, D. E., and S. Chu, ''Response of flexible polymers to a sudden elongational flow,'' Science **281**, 1335–1340 (1998).
Tirtaatmadja, V. and T. Sridhar, ''Comparison of constitutive equations of polymer solutions in uniaxial extension,'' J. Rheol. **39**, 1133–1159 (1995).
van den Brule, B. H. A. A., ''Brownian dynamics simulation of finitely extensible bead-spring chains,'' J. Non-Newtonian Fluid Mech. **47**, 357–378 (1993).
Verhoef, M. R. J., B. H. A. A. van den Brule, and M. A. Hulsen, ''On the modeling of PIB/PB Boger Fluid in extensional flow,'' J. Non-Newtonian Fluid Mech. **80**, 155–182 (1999).
Wedgewood, L. E., D. N. Ostrov, and R. B. Bird, ''A finitely extensible bead-spring chain model for dilute polymer solutions,'' J. Non-Newtonian Fluid Mech. **40**, 119–139 (1991).
Wiest, J. M., ''Birefringence in strong flows of dilute polymer solutions,'' Polymer **40**, 1917–1922 (1998).
Wiest, J. M. and R. I. Tanner, ''Rheology of bead-nonlinear spring chain macromolecules,'' J. Rheol. **33**, 281–316 (1989).